

CONFIDENTIAL

RM L53H17

NACA RM L53H17



RESEARCH MEMORANDUM

INVESTIGATION OF THE EFFECT OF SPANWISE
POSITIONING OF A VERTICALLY SYMMETRIC OGIVE-CYLINDER
NACELLE ON THE HIGH-SPEED AERODYNAMIC CHARACTERISTICS
OF A 45° SWEEPBACK TAPERED-IN-THICKNESS

WING OF ASPECT RATIO 6 WITH
AND WITHOUT A FUSELAGE

By H. Norman Silvers and Thomas J. King, Jr.

Langley Aeronautical Laboratory
Langley Field, Va.

CLASSIFIED DOCUMENT

This material contains information affecting the National Defense of the United States within the meaning of the espionage laws, Title 18, U.S.C., Secs. 793 and 794, the transmission or revelation of which in any manner to an unauthorized person is prohibited by law.

NATIONAL ADVISORY COMMITTEE FOR AERONAUTICS

WASHINGTON
October 7, 1953

CLASSIFICATION CHANGED

UNCLASSIFIED

To

By

NACA Rec also

Authority of XRN-119

Amr 9-5-57

effective Aug 16 1957

CONFIDENTIAL



NATIONAL ADVISORY COMMITTEE FOR AERONAUTICS

RESEARCH MEMORANDUM

INVESTIGATION OF THE EFFECT OF SPANWISE
POSITIONING OF A VERTICALLY SYMMETRIC OGIVE-CYLINDER
NACELLE ON THE HIGH-SPEED AERODYNAMIC CHARACTERISTICS
OF A 45° SWEEPBACK TAPERED-IN-THICKNESS
WING OF ASPECT RATIO 6 WITH
AND WITHOUT A FUSELAGE

By H. Norman Silvers and Thomas J. King, Jr.


SUMMARY

An ogive-cylinder nacelle was investigated in various spanwise locations in a vertically symmetric position on a small-size 45° sweptback wing of aspect ratio 6 with and without a fuselage. Comparisons were made between these results and results obtained in another investigation of an underwing nacelle to show the effect of nacelle vertical position. The Mach number range of this investigation extended from 0.70 to 1.08.

The results indicate that the changes in installation drag due to changes in nacelle spanwise position in general conformed to the concepts of the transonic area rule. In regard to nacelle vertical position, however, the symmetrical nacelle had measurably lower installation drag than the underwing nacelle in spite of only minor differences in the area development of the model-nacelle combination. Furthermore, fuselage-induced interference increased the drag of the symmetrical nacelle installation at intermediate spanwise locations but decreased the drag of extreme inboard and wing-tip locations of this arrangement. Some significant effects of the variables investigated on lift-curve slope, stability characteristics, and the loading characteristics of the model (indicated by measurement of the lateral-center-of-pressure locations) also are indicated.

INTRODUCTION

The National Advisory Committee for Aeronautics is conducting a program of research on nacelles and external stores in order to provide installations suitable for use on airplanes at transonic speeds. The



investigations of this program are concerned with an overall evaluation of the effects of body positioning and shape on the aerodynamic characteristics of models with straight and sweptback wings.

The present paper is the third in a series of papers reporting the results of investigations made in the Langley high-speed 7- by 10-foot tunnel as part of the general program. In the present paper are presented results showing the effect of spanwise positioning of a vertically symmetric ogive-cylinder nacelle on a 45° sweptback wing with and without a fuselage. Also included in this paper is a comparison between the present results and those obtained with an underwing mounting of the nacelle (ref. 1) to show the effect of nacelle vertical position. The effect of chordwise positioning of underwing nacelles of three profile shapes on a 45° sweptback wing without a fuselage are presented in reference 2.

In the investigations of nacelles made in the 7- by 10-foot tunnel (refs. 1 and 2), as well as those made earlier by the Pilotless Aircraft Research Division (refs. 3 to 7), a wing of 45° sweepback, aspect ratio 6, taper ratio 0.6, and NACA 65A-series airfoil sections has been used as the test vehicle. The thickness of the wing used in the tunnel investigations tapered from 9 percent at the root to 3 percent at the tip, while the wing of the flight models was 9 percent thick from root to tip.

For the most part, the bodies used in these investigations have been solid; however, in reference 7, the effects of internal flow on the drag characteristics of the model are presented for one configuration of the nacelle. In reference 8, results which were obtained in the Langley 8-foot transonic tunnel are presented for several configurations of ducted nacelles.

SYMBOLS

C_L	lift coefficient, Twice semispan lift/ qS_w
C_D	drag coefficient, Twice semispan drag/ qS_w
C_{D_n}	nacelle-drag coefficient, $(C_{D_{\text{model+nacelle}}} - C_{D_{\text{model}}}) \frac{S_w}{2S_n}$
C_m	pitching-moment coefficient referred to $0.25\bar{c}$ of wing, Twice semispan pitching moment/ $qS_w\bar{c}$
C_B	bending-moment coefficient, Twice root bending moment/ $qS_w \frac{b}{2}$

q	free-stream dynamic pressure, $1/2\rho V^2$, lb/sq ft
S_w	twice area of semispan model, 0.125 sq ft
S_n	maximum frontal area of nacelle, 0.00119 sq ft
\bar{c}	mean aerodynamic chord of wing, 0.147 ft, $\frac{2}{S_w} \int_0^{b/2} c^2 dy$ (using theoretical tip)
c	local wing chord parallel to chord plane
b	twice span of semispan model, 0.866 ft
d_f	fuselage diameter
d_n	nacelle diameter
x	longitudinal distance from wing leading edge to nose of nacelle; negative when nose of nacelle is forward of wing leading edge
y	lateral distance from plane of symmetry to center line of nacelle
l_f	fuselage length
l_n	nacelle length
V	effective free-stream air velocity
M	effective free-stream Mach number, $\frac{2}{S_w} \int_0^{b/2} c M_a dy$
M_l	local Mach number
M_a	average chordwise Mach number
ρ	mass density of air
α	angle of attack, deg

y_{cp} lateral center of pressure referred to wing semispan, $\frac{\partial C_B}{\partial C_L}$

$$C_{L\alpha} = \left(\frac{\partial C_L}{\partial \alpha} \right)_M$$

$$C_{mC_L} = \left(\frac{\partial C_m}{\partial C_L} \right)_M$$

APPARATUS AND MODELS

This investigation utilized a small-size semispan model that was mounted on a reflection-plane plate, located 3 inches from the tunnel wall in order to bypass the wall boundary layer (fig. 1). A more detailed discussion of the model setup and the strain-gage balance system employed, is given in reference 1.

The wing was constructed of steel with 45° sweepback referred to the quarter-chord line, aspect ratio 6, and a taper ratio of 0.6. The airfoil sections parallel to the free stream were NACA 65A-series sections that tapered in thickness from 9 percent at the root chord to 3 percent at the theoretical tip chord.

The fuselage was made of brass and was mounted to the wing so that there was a clearance gap of $1/32$ of an inch between the reflection plane plate and the inside surface of the fuselage. With the fuselage in place, the nominal panel span of the wing was therefore reduced by $1/32$ of an inch. Ordinates of the fuselage are presented in table I.

The fuselage used in this investigation consisted of a body formed by ogival nose and tail sections having a basic fineness ratio of 12. For testing, a section of the tail was removed to form a blunt-ended body of fineness ratio 10. The fuselage of references 3 to 7 has a nose section similar to the present fuselage in that both utilized a section generated by revolution of an ogival arc. The nose section of the fuselage of references 3 to 7 was slightly longer in proportion to the maximum diameter than that of the fuselage used in this investigation. In contrast to the continuously varying curvature of the present fuselage tail section, the tail section contour of the fuselage of references 3 to 7 was formed by locating a straight-line element so as to be tangent to the fuselage contour somewhat behind the maximum diameter. This resulted in a larger base diameter of the tail section of the fuselage of the

reference papers than that of the present fuselage. On both fuselages, the wings were located so that the leading edges intersected the fuselage maximum diameter at the surface of the fuselage.

The nacelle was a solid body of revolution constructed of mahogany. The nacelle shape consisted of ogival nose and tail sections and a cylindrical midsection. Nacelle ordinates are presented in table II. The nacelle fineness ratio was 9.34. The nacelle was located along the wing chord line so that the midlength of the hypothetical ducted body as discussed in reference 2 would lie on the 0.5-chord line of the wing. A drawing showing the nacelle locations is presented in figure 2. Four spanwise locations of the nacelle were investigated: $0.20b/2$, $0.46b/2$, $0.70b/2$, and $0.96b/2$. Results for two vertical locations of the nacelle are compared in this paper for each spanwise location on the wing without a fuselage. They were a symmetrical position where the nacelle center line lay in the chord plane of the wing and an underwing position where the nacelle center line was one-half the maximum diameter below the chord plane of the wing. Results of the latter configuration have been reported earlier in reference 1. The vertically symmetric nacelle was also investigated in each spanwise location with the fuselage in position on the wing.

The ogive-cylinder nacelle of this investigation was similar in shape to the nacelle investigated in references 3 to 7, in that for both nacelles ogival nose and tail sections were used between which was located a cylindrical length of body. For the nacelle of the present investigation, the ogival tail section terminated in a point while the nacelles of references 3 to 7 were blunt ended; that is, a portion of the ogival tail was removed. The fineness ratio of the nacelle used herein was 9.34, while that of the nacelle of references 3 to 7 was 9.66.

The nacelle used herein was also somewhat larger relative to the wing than were the nacelles of the flight investigations. The size of the nacelle of this investigation was determined from existing jet-engine specifications and by considering the wing to be a 0.01-scale model of a bomber wing. At full scale the diameter of the nacelle would be about 47 inches and the airplane would be of the medium-bomber category.

METHODS AND TESTS

The reflection-plane plate attached to the wall of the Langley high-speed 7- by 10-foot tunnel induces over its surface a region of local velocities higher than the free-stream velocities of the tunnel, which permits testing of small models to Mach numbers of 1.08. The variations in local Mach number over the reflection-plane plate are shown in figure 3 for typical Mach numbers. As indicated by these data, the Mach

number gradient in the region of the model decreases with decreasing tunnel speed. At a Mach number of about 0.93, the flow is gradient free. Effective free-stream Mach numbers which are used as the basis of data presentation were obtained from the relationship

$$M = \frac{2}{S_w} \int_0^{b/2} cM_a dy$$

Lift, drag, pitching-moment, and bending-moment coefficients were measured over an angle-of-attack range that extended from about -1.5° to 9.0° at Mach numbers from 0.70 to 1.08. The variation of Reynolds number with Mach number for these tests is shown in figure 4. Because of the small size of the model employed in this investigation, jet boundary and blockage corrections were considered negligible.

In general, the accuracy of the force and moment measurements can be judged by any random scatter of the test points of the basic data. In determining increments of forces and moments, however, faired values of forces and moments are used, thus tending to minimize the influence of test-point scatter on the curves of the summary results.

Experience with the technique of locating small reflection-plane models in a localized high-velocity field to obtain transonic speeds has indicated that absolute values of coefficients, particularly drag, may not correlate well with data obtained on larger complete models. Valid incremental effects, such as those due to model configuration, lift coefficient, or Mach number are, however, felt to be obtained by this technique. These conclusions were reached after correlative studies of results from bump-type test techniques and the conventional sting-type test techniques had been made (for example, ref. 9).

RESULTS AND DISCUSSION

The results of this investigation are presented in the figures, the content of which is summarized below.

	Figure
Basic data:	
Wing alone	5
Wing fuselage	6
Wing with symmetrical nacelle	7
Wing fuselage with symmetrical nacelle	8
Wing with underwing nacelle	9
Drag characteristics	10 to 15
Summary of aerodynamic characteristics	16 to 23

Lift-curve slopes presented were measured through zero lift while pitching-moment-curve slopes were measured at a lift coefficient of 0.1.

Drag Characteristics

The drag coefficients as a function of Mach number have been obtained on the models with and without the nacelle in the various test locations and the results are presented in figure 10. From these data, the increments in drag due to the nacelle have been taken and the results, based on the nacelle frontal area and called "nacelle drag coefficient," are presented in figure 11 as a function of Mach number, in figure 12 as a function of lift coefficient, and in figure 13 as a function of nacelle spanwise location.

Although underwing mounting of nacelles is preferred by many manufacturers, the drag of such installations is generally higher than the drag of the vertically symmetric installation throughout the Mach number range over a large part of the lift-coefficient range. Similar drag characteristics have been shown in flight investigations made at zero lift (ref. 3) at Mach numbers up to about 1.25. A part of the additional drag of the underwing installation probably is due to poor flow characteristics in the wing-nacelle junctures which has been discussed in reference 1.

Fuselage interference has an appreciable effect on the drag coefficients of the symmetrical nacelle, producing an increase in C_{D_n} for the intermediate spanwise locations of the nacelle, and at the lower lift coefficients resulting in a reduction in C_{D_n} for the wing-tip location. At the higher lift coefficients fuselage interference does not show a consistent effect on the drag of the tip nacelle.

Because of the significance of fuselage interference on the nacelle drag coefficients of this investigation, it should be emphasized that although the fuselage used is a standardized research shape, it is not necessarily intended to simulate interference effects either at subsonic or transonic speeds that would be obtained by a particular type of airplane fuselage.

In connection with fuselage as well as nacelle interference it is of interest to inspect some of the drag results presented in this paper from the standpoint of a method (ref. 10) that proposes a way of estimating the comparative levels of drag at transonic speeds. Reference 10 indicates that the area development along the length of the model in a plane perpendicular to the plane of symmetry may provide an index to the increase in drag that occurs in going from subsonic to transonic speeds. The different

locations of the nacelle of this investigation, because of the wing sweep, result in some significant changes in the area development.

Several arrangements of the nacelle have been selected to illustrate the development of area (fig. 14) and the increment in drag has been taken between the drag at Mach numbers greater than 0.9 and the drag at 0.9 for these configurations at zero lift coefficient. The results show that the increase in drag coefficient at transonic speeds is a function of the increase in maximum cross-sectional area of the configuration. Any reduction of the maximum area by repositioning of the nacelle or reduction of the maximum area by removal of the fuselage reduces the drag level at Mach numbers near 1.0. It is to be noted that there is some difference in transonic drag between the symmetrical and the underwing nacelle on the wing without the fuselage in spite of an insignificant change in the maximum area of these arrangements. It would appear that such a refinement in interpretation of the area developments is not justified. It is also to be noted that while the addition of the tip nacelle did not increase the maximum area, it did result in an irregularly shaped distribution. It would appear that lower drag might have been attained with this location had the models been shaped to provide a smooth area development. In general, though, the method of reference 10 applied to the results of this investigation gives a good indication of the comparative levels of drag at transonic speeds for the model and nacelle arrangements used.

It is possible that any reflection-plane disturbances due to boundary layer or shock reflections may be of significance in nacelle drag coefficient. To indicate possible reflection-plane effects, a comparison is made in figure 15 between some of the results presented in this paper and results obtained on similar but larger complete models in flight (refs. 3 and 5). This comparison is made at zero lift, the lift coefficient of the flight results, and at two Mach numbers which show representative nacelle drag for the subsonic and low supersonic speed ranges. The agreement between the results is qualitatively good at a Mach number of 1.08, thus indicating that at transonic speeds, the reflection plane does not have any major effect upon the changes in the nacelle drag coefficients due to change in nacelle spanwise location. The level of nacelle drag coefficients of the semispan model is, however, somewhat higher for all spanwise locations of nacelle than the nacelle drag coefficients of the larger complete models — a result discussed in more detail in reference 9. At a Mach number of 0.90, the agreement between the results is poor. The accuracy of nacelle drag measurements obtained by both test techniques is, however, not so good at the lower speeds as it is at the higher speeds.

Lift-Drag Ratios

The variations in maximum lift-drag ratios of the models without nacelles and for the models with nacelles in the various test locations are presented in figure 16. A convenient quantitative expression of the effect of the nacelles on the maximum lift-drag ratios of the models is given by the ratio of the $(L/D)_{\max}$ of the model with nacelles to the $(L/D)_{\max}$ of the model without nacelles. These ratios are summarized in figure 17. The ratio gives values greater than 1.0 if the maximum lift-drag ratio of the model with nacelle is higher than that for the model without nacelle.

The highest ratios of maximum lift-drag ratio were obtained at subsonic Mach numbers for the symmetrical nacelle on the wing without a fuselage over most of the nacelle spanwise range. Comparison of these results with those obtained with the fuselage in place indicates that, at subsonic Mach numbers, fuselage interference has an adverse effect on the ratio of $(L/D)_{\max}$ for intermediate spanwise locations of the nacelle. At a supersonic Mach number of 1.08, fuselage interference becomes favorable.

The largest effect of nacelle spanwise location on the ratios of $(L/D)_{\max}$ was obtained at subsonic speeds for the symmetrical nacelle on the wing-fuselage combination. For this configuration the ratios of $(L/D)_{\max}$ were the lowest at a nacelle location of $0.46b/2$ and the highest at nacelle locations of $0.96b/2$ and $0.20b/2$. At a Mach number of 0.70, the ratios became slightly greater than 1.0. This is of course related to the low nacelle drag coefficients shown earlier for this configuration of nacelle and model. The low drag and high $(L/D)_{\max}$ at subsonic speeds of the symmetrical nacelle at $0.96b/2$ that were obtained not only on the wing-fuselage combination but also on the wing alone are a result of the nacelle's acting as a wing end plate. The underwing nacelle at the wing tip does not show any evidence of acting as a wing end plate.

Increase in Mach number reduces the ratios of $(L/D)_{\max}$ of the best configurations of nacelles (extreme inboard and tip locations of the symmetrical nacelle on the wing-fuselage model). The reductions are equivalent to a reduction in the ratios of $(L/D)_{\max}$ of 10 percent for the inboard location and about 17 percent for the extreme tip location.

Lift Characteristics

The increments in slopes of the lift curves due to the nacelle in the various spanwise locations have been obtained from figure 18 and are presented in figure 19.

Positive increases in $C_{L\alpha}$ of the model due to the nacelles were generally obtained at subsonic speeds with the largest increases being shown for the underwing nacelle in most nacelle spanwise locations. This configuration also resulted in the highest increments in lift-curve slope for outboard locations at a Mach number of 1.08. Nacelle spanwise location showed some pronounced effects on $\Delta C_{L\alpha}$ for the underwing nacelle. The effects of both spanwise and chordwise location of the underwing nacelle are more fully discussed in reference 1. The fuselage reduced the increment in lift-curve slope for the symmetrical nacelle at almost all nacelle spanwise locations.

Pitch Characteristics

The slopes of the pitching-moment curves taken at a lift coefficient of 0.1 are presented in figure 20 for the models without and with the nacelles in the test locations. Increments in the pitching-moment-curve slopes due to the nacelles are presented in figure 21. The slopes of the pitching-moment curves obtained at $C_L = 0.1$ indicate some rather erratic effects of the several variables investigated. Some of the largest changes in the increment in slope of the pitching-moment curves come from changes in nacelle spanwise location. At a Mach number of 1.08, change in spanwise location of the symmetrical nacelle on the wing alone results in the largest change which is equivalent to a change in the aerodynamic-center location of more than 11 percent of the mean aerodynamic chord. The average change, however, for all Mach numbers and nacelle arrangements appears to be equivalent to from 5 to 7 percent change in aerodynamic-center location based on the mean aerodynamic chord.

At the higher lift coefficients, a destabilizing break develops in the pitching-moment curves for the wing alone and the wing-fuselage combination at Mach numbers of about 1.05 and lower (figs. 5 and 6). Intermediate spanwise locations ($0.46b/2$ and $0.70b/2$) of the symmetrical and the underwing nacelle extend the lift-coefficient range where the unstable break occurs (figs. 7 and 9). Intermediate locations of the symmetrical nacelle also extend the range for the destabilizing break of the wing-fuselage combination, but only at the lower Mach numbers (fig. 8). On the other hand, the tip mounting ($0.96b/2$) of the symmetrical nacelle on the wing-fuselage combination produces an unstable pitching-moment break at even lower lift coefficients than for the wing-fuselage combination without the nacelle.

Lateral Center of Pressure

The lateral centers of pressure are presented in figure 22 for the models with and without nacelles. The incremental changes in the lateral centers of pressure have been determined and are presented in figure 23. The changes in the location of the lateral center of pressure due to changes in the independent variables of this investigation are appreciable. Spanwise and vertical position of the nacelle each makes as much as a 6-percent change in the locations of the lateral center of pressure. Changes of this order of magnitude indicate that the nacelles can have a significant effect on the loading characteristics of the wing panel.

CONCLUSIONS

An investigation of the high-speed aerodynamic effects of spanwise positioning of an underwing and vertically symmetric ogive-cylinder nacelle on a small-size 45° sweptback wing and the effects of a vertically symmetric ogive-cylinder nacelle on the wing combined with a fuselage indicate the following conclusions:

1. The changes in installation drag due to changes in nacelle spanwise position in general conformed to the concepts of the transonic area rule. In regard to nacelle vertical position, however, the symmetrical nacelle had measurably lower installation drag than the underwing nacelle in spite of only minor differences in the area development.
2. Fuselage-induced interference increased the installation drag of the symmetrical nacelle at intermediate spanwise locations, but decreased the drag of extreme wing-tip locations of this configuration.
3. Nacelle spanwise location, vertical position, and fuselage-induced interference all showed significant effects on the lift-curve slope and the stability characteristics of the model as well as on the loading characteristics of the wing as indicated by the lateral-center-of-pressure measurements.

Langley Aeronautical Laboratory,
National Advisory Committee for Aeronautics,
Langley Field, Va., August 14, 1953.

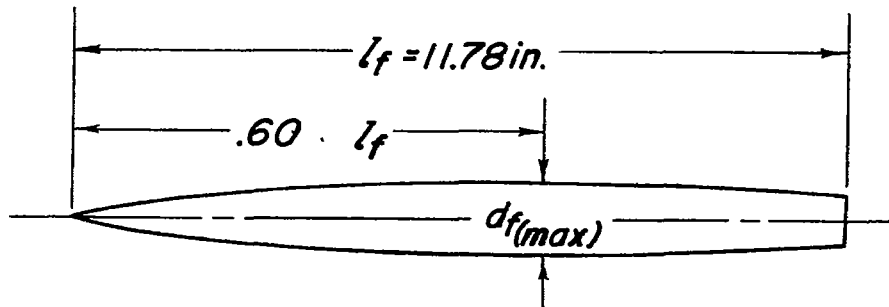
REFERENCES

1. Silvers, H. Norman, and King, Thomas J., Jr.: A Small-Scale Investigation of the Effect of Spanwise and Chordwise Positioning of an Ogive-Cylinder Underwing Nacelle on the High-Speed Aerodynamic Characteristics of a 45° Sweptback Tapered-in-Thickness Wing of Aspect Ratio 6. NACA RM L52J22, 1952.
2. Silvers, H. Norman, and King, Thomas J., Jr.: Investigation of the Effect of Chordwise Positioning and Shape of an Underwing Nacelle on the High-Speed Aerodynamic Characteristics of a 45° Sweptback Tapered-in-Thickness-Ratio Wing of Aspect Ratio 6. NACA RM L52K25, 1953.
3. Pepper, William B., Jr., and Hoffman, Sherwood: Transonic Flight Tests To Compare the Zero-Lift Drag of Underslung and Symmetrical Nacelles Varied Chordwise at 40 Percent Semispan of a 45° Sweptback, Tapered Wing. NACA RM L50G17a, 1950.
4. Pepper, William B., Jr., and Hoffman, Sherwood: Comparison of the Zero-Lift Drags Determined by Flight Tests at Transonic Speeds of Symmetrically Mounted Nacelles in Various Spanwise Positions on a 45° Sweptback Wing and Body Combination. NACA RM L51D06, 1951.
5. Hoffman, Sherwood: Comparison of Zero-Lift Drag Determined by Flight Tests at Transonic Speeds of Pylon, Underslung, and Symmetrically Mounted Nacelles at 40 Percent Semispan of a 45° Sweptback Wing and Body Combination. NACA RM L51D26, 1951.
6. Hoffman, Sherwood: Transonic Flight Tests To Compare the Zero-Lift Drags of Underslung Nacelles Varied Spanwise on a 45° Sweptback Wing and Body Combination. NACA RM L52D04a, 1952.
7. Hoffman, Sherwood, and Pepper, William B., Jr.: Transonic Flight Tests To Determine Zero-Lift Drag and Pressure Recovery of Nacelles Located at the Wing Tips on a 45° Sweptback Wing and Body Combination. NACA RM L51K02, 1952.
8. Bielat, Ralph P., and Harrison, Daniel E.: A Transonic Wind-Tunnel Investigation of the Effects of Nacelle Shape and Position on the Aerodynamic Characteristics of Two 47° Sweptback Wing-Body Configurations. NACA RM L52G02, 1952.
9. Donlan, Charles J., Myers, Boyd C., II, and Mattson, Axel T.: A Comparison of the Aerodynamic Characteristics at Transonic Speeds of Four Wing-Fuselage Configurations as Determined From Different Test Techniques. NACA RM L50H02, 1950.

10. Whitcomb, Richard T.: A Study of the Zero-Lift Drag-Rise Characteristics of Wing-Body Combinations Near the Speed of Sound. NACA RM L52H08, 1952.

TABLE I. - FUSELAGE ORDINATES

[Basic fineness ratio 12, actual fineness ratio
10 achieved by cutting off rear portion of body]

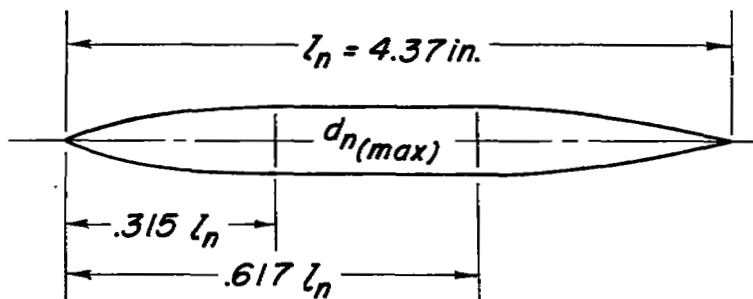


Ordinates, percent length	
Station	Radius
0	0
.60	.28
.90	.36
1.50	.51
3.00	.87
6.00	1.45
9.00	1.94
12.00	2.37
18.00	3.11
24.00	3.71
30.00	4.16
36.00	4.49
42.00	4.72
48.00	4.88
54.00	4.97
60.00	5.00
66.00	4.96
72.00	4.83
78.00	4.61
84.00	4.28
90.00	3.75
96.00	3.03
100.00	2.50

L. E. radius = .0006 l_f

TABLE II.- NACELLE ORDINATES

[Fineness ratio 9.34]



Ordinates, percent length	
Station	Radius
0	0
.36	.30
1.21	.73
3.04	1.44
4.87	2.09
6.71	2.65
8.26	3.07
9.15	3.29
9.69	3.44
10.84	3.70
11.99	3.94
13.14	4.12
14.29	4.30
15.44	4.44
17.74	4.70
20.04	4.92
22.34	5.08
24.64	5.20
26.94	5.30
29.24	5.34
31.54	5.36
61.70	5.36
68.69	5.20
74.95	4.76
81.22	3.94
87.48	2.76
90.60	2.11
93.75	1.42
96.89	.72
98.44	.36
100.00	0

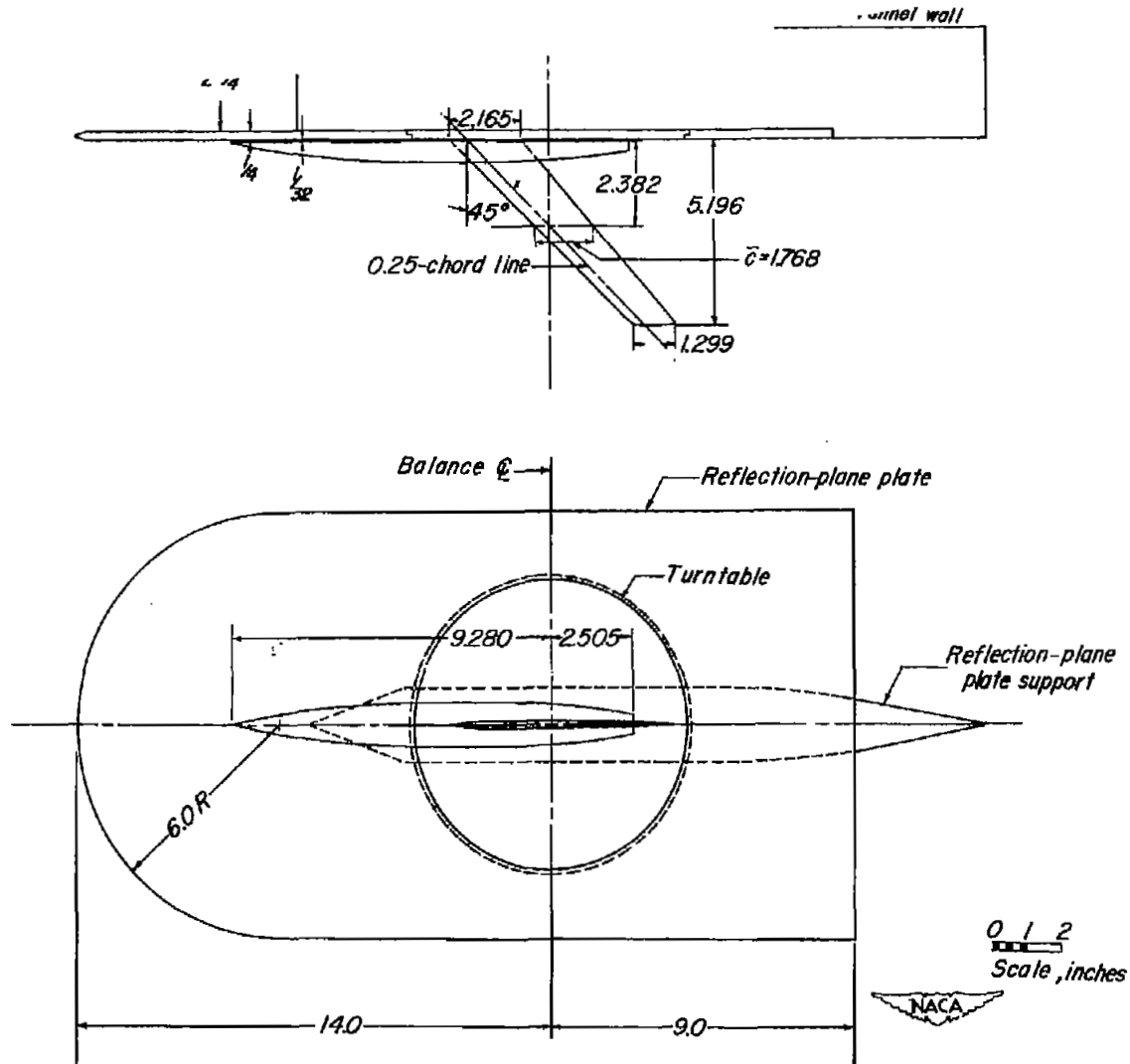
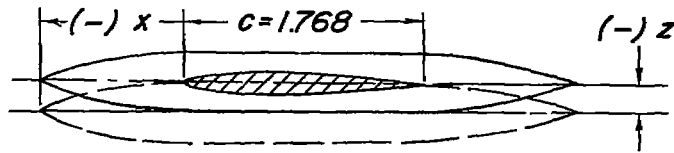
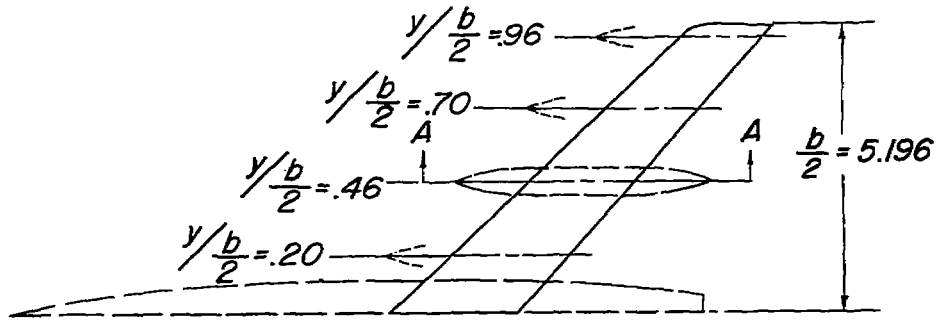


Figure 1.- Two-view drawing of the test setup.



Section A - A

Nacelle location		
$y/\frac{b}{2}$	x/c	$z/d_{n(max)}$
.20	-556	0
.46	-698	0
.70	-859	0
.96	-1.083	0
.20	-556	-.50
.46	-698	-.50
.70	-859	-.50
.96	-1.083	-.50



Figure 2.- Nacelle locations.

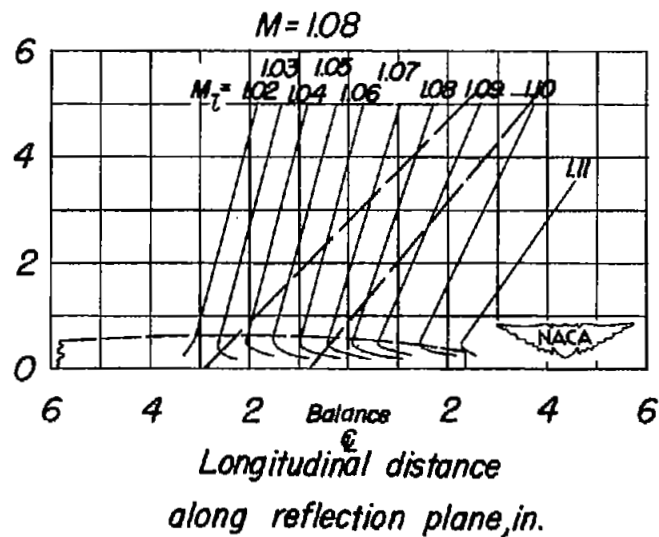
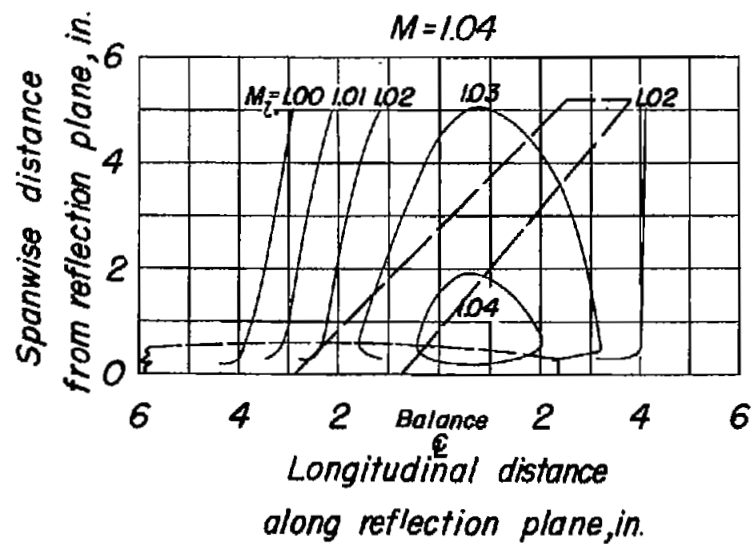
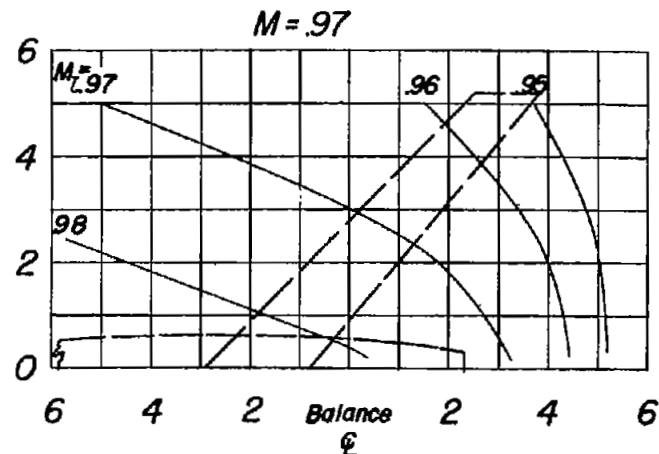
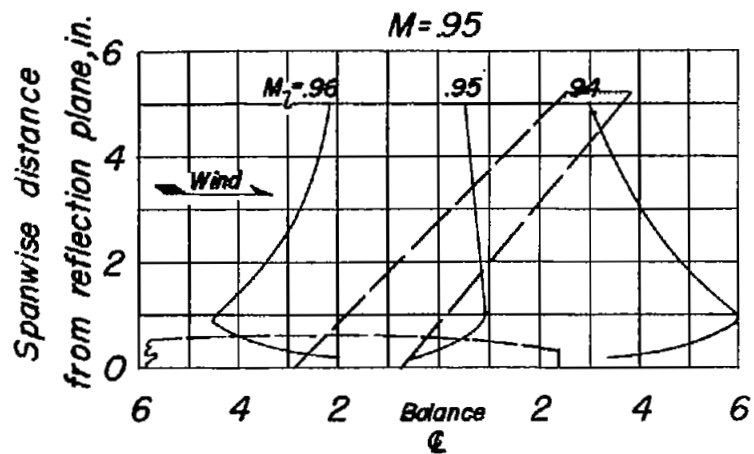


Figure 3.- Typical Mach number contours over side-wall reflection plane in region of model location.

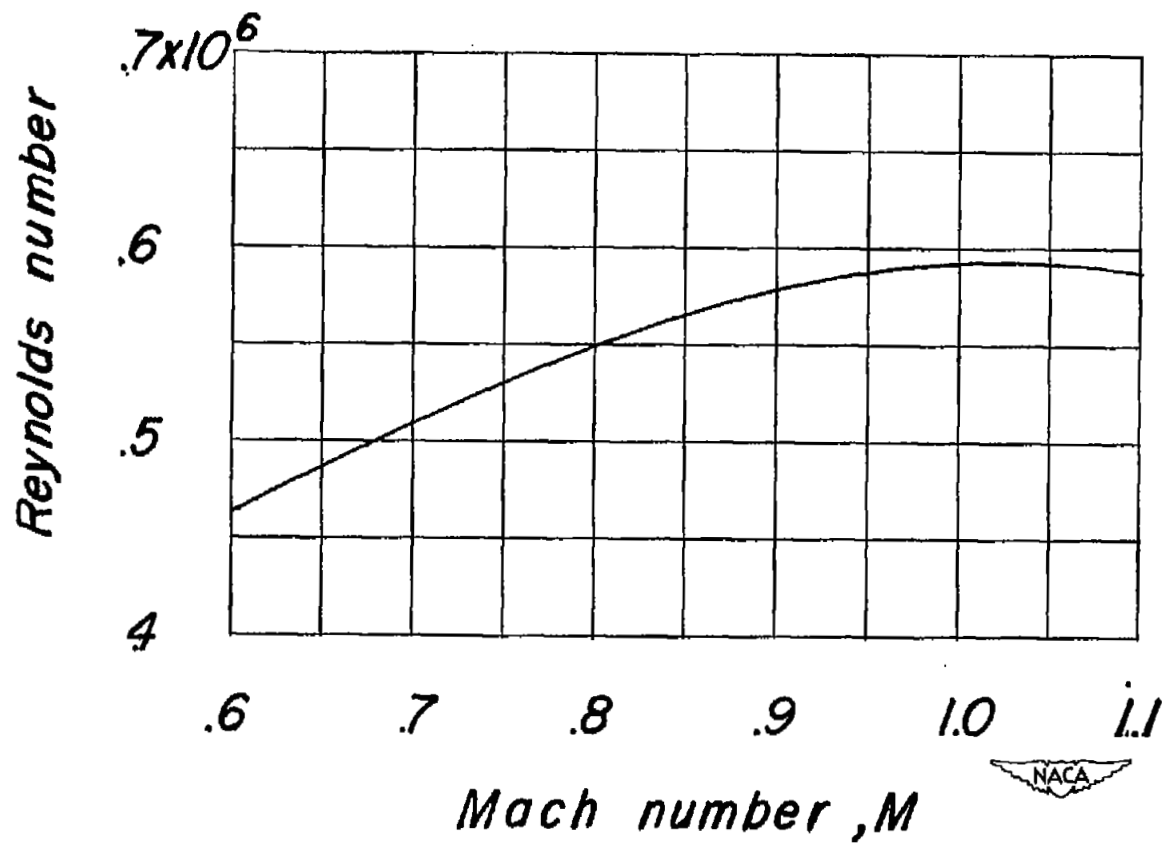


Figure 4.- Variation of Reynolds number with Mach number for the model in the Langley high-speed 7- by 10-foot tunnel.

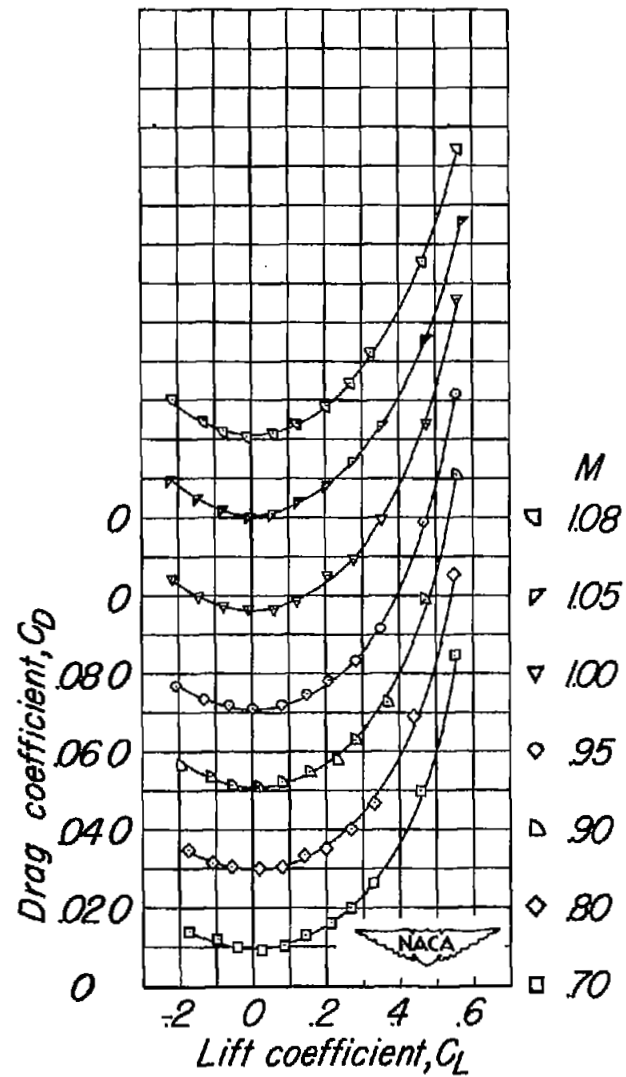
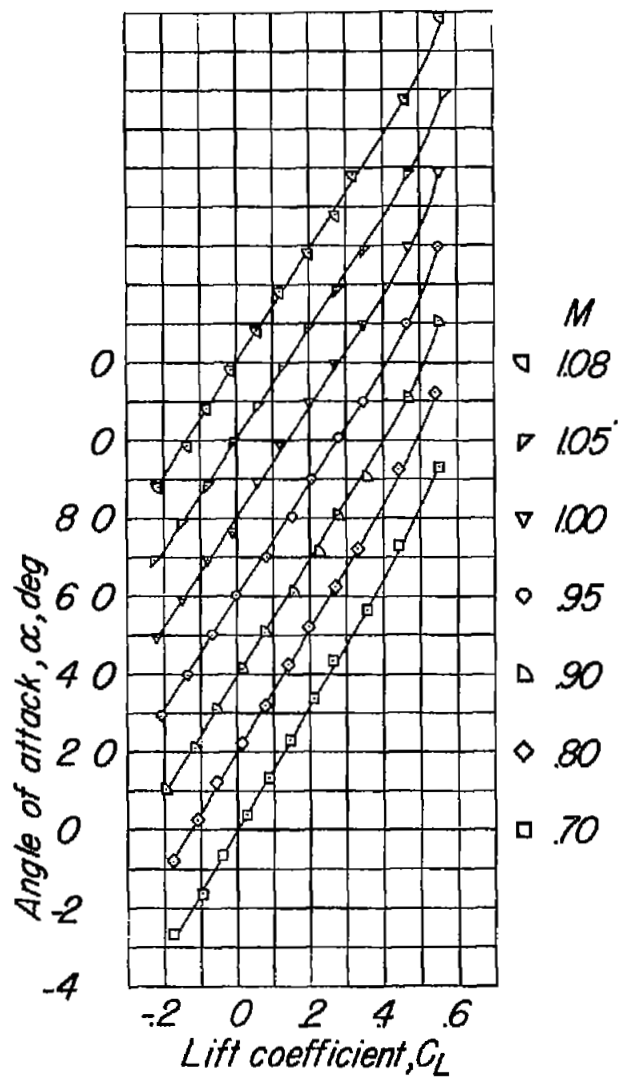


Figure 5.- Aerodynamic characteristics of the semispan wing.

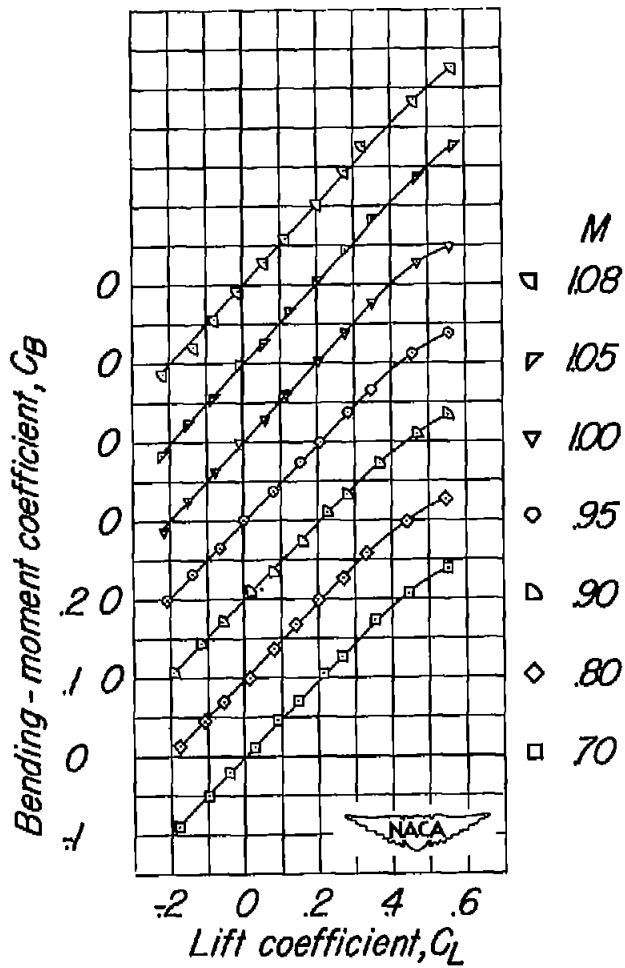
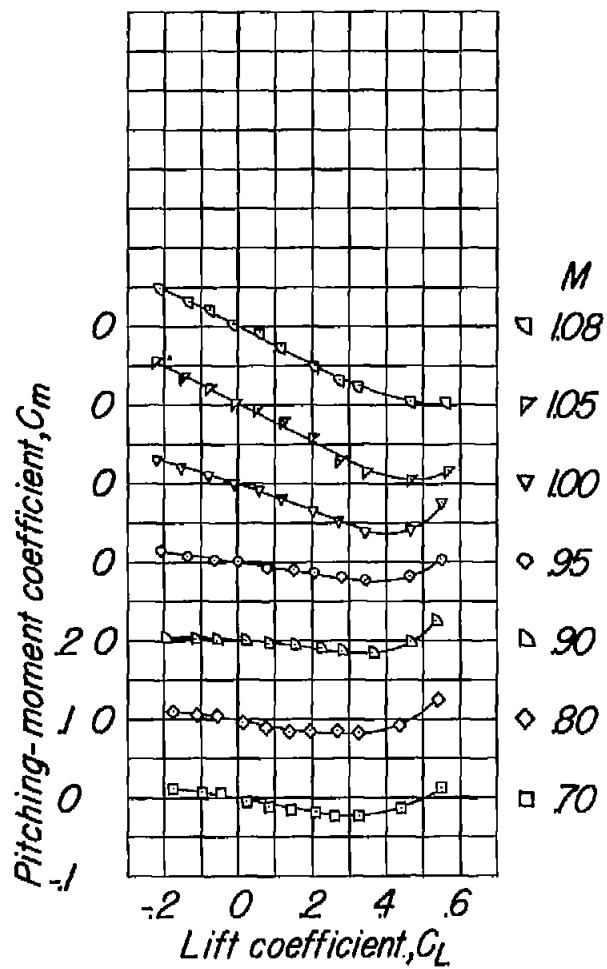


Figure 5.- Concluded.

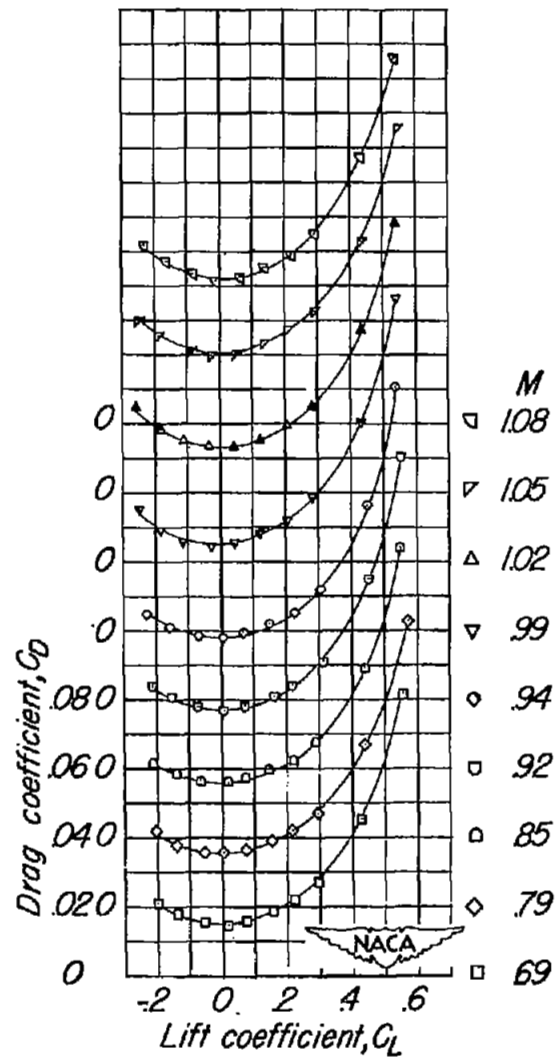
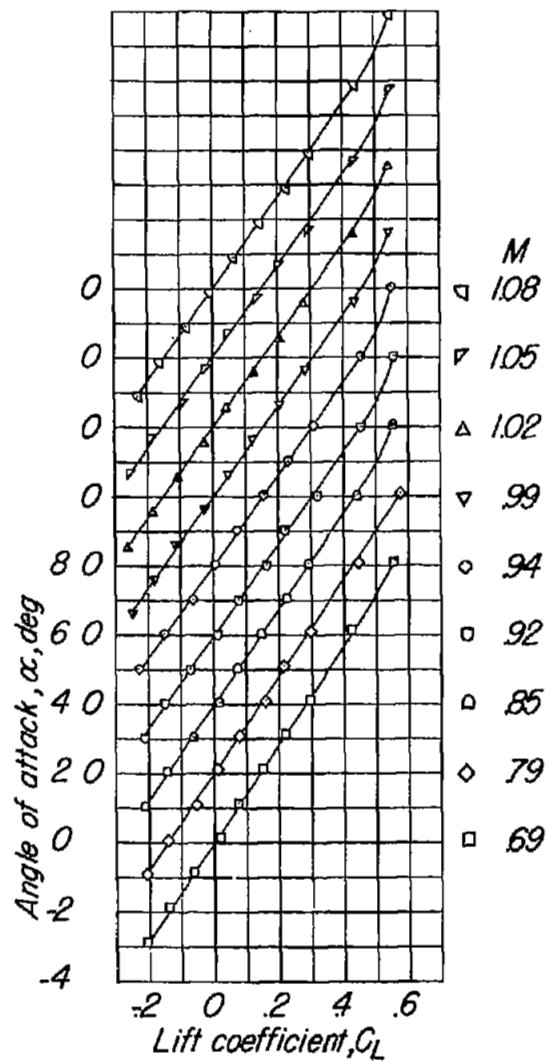


Figure 6.- Aerodynamic characteristics of the semispan wing combined with the fuselage.

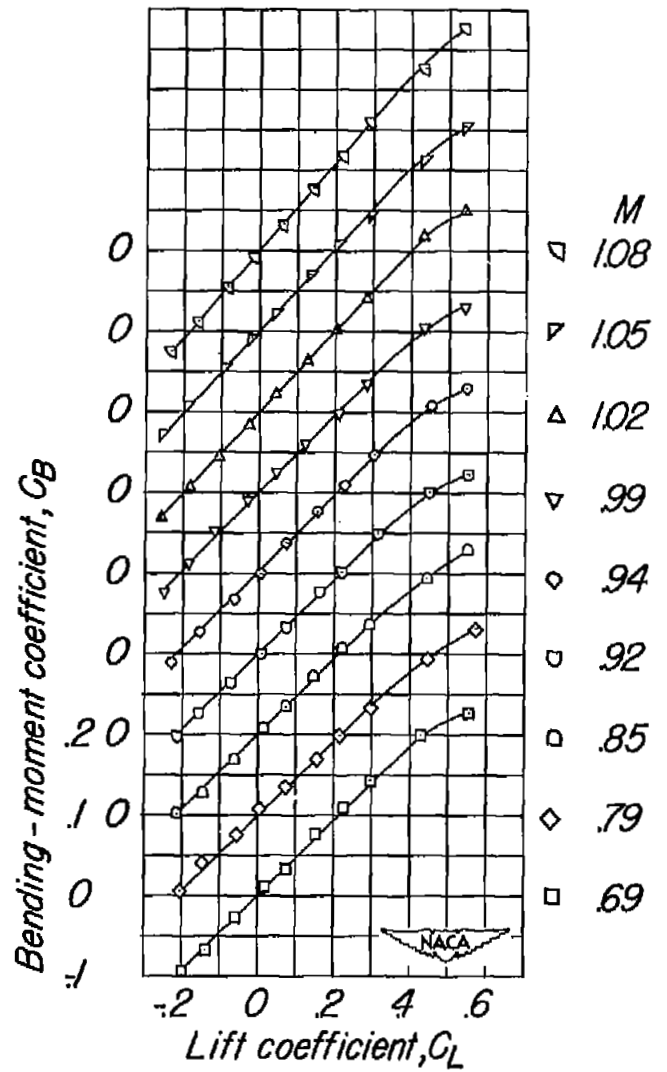
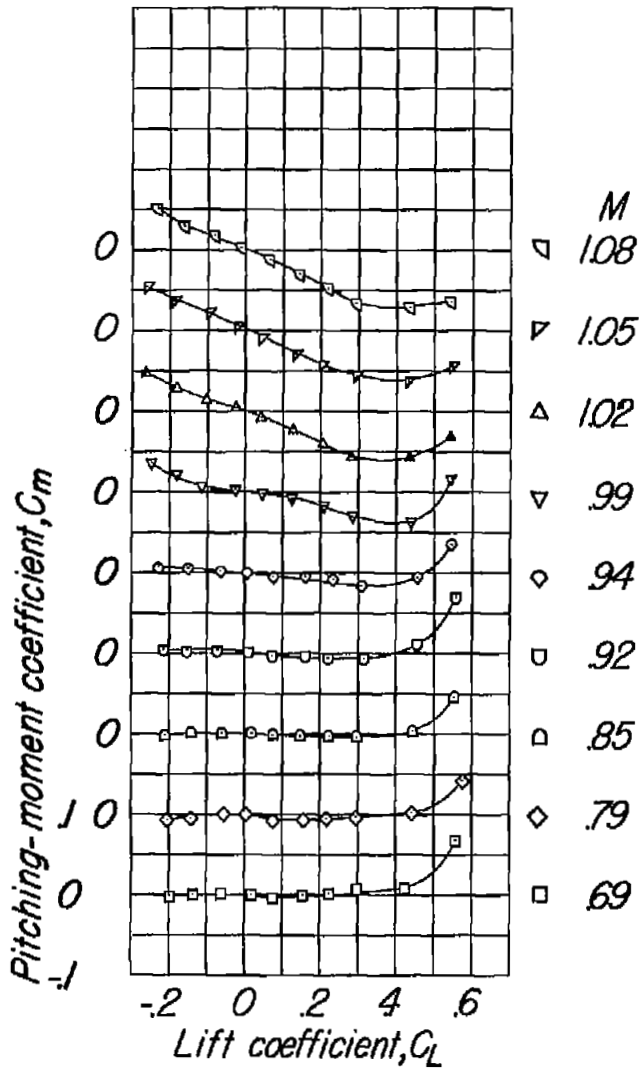
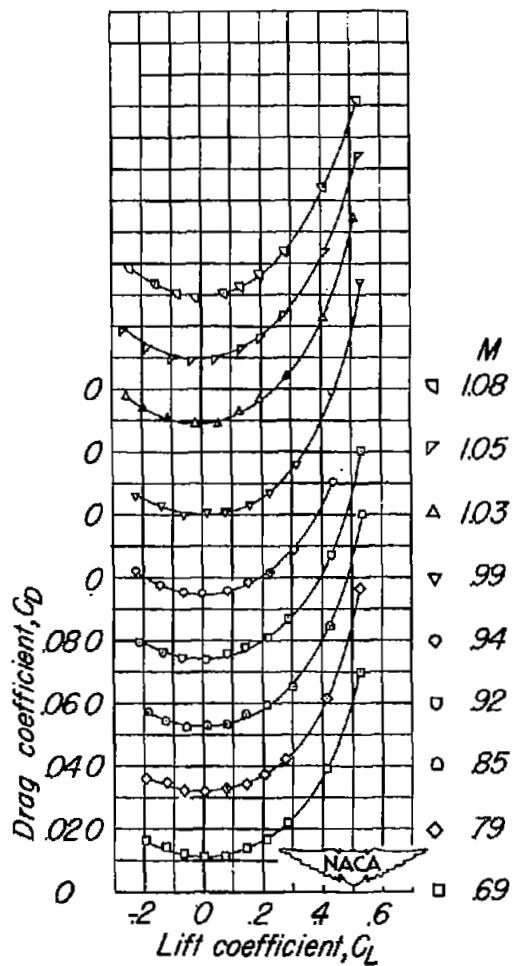
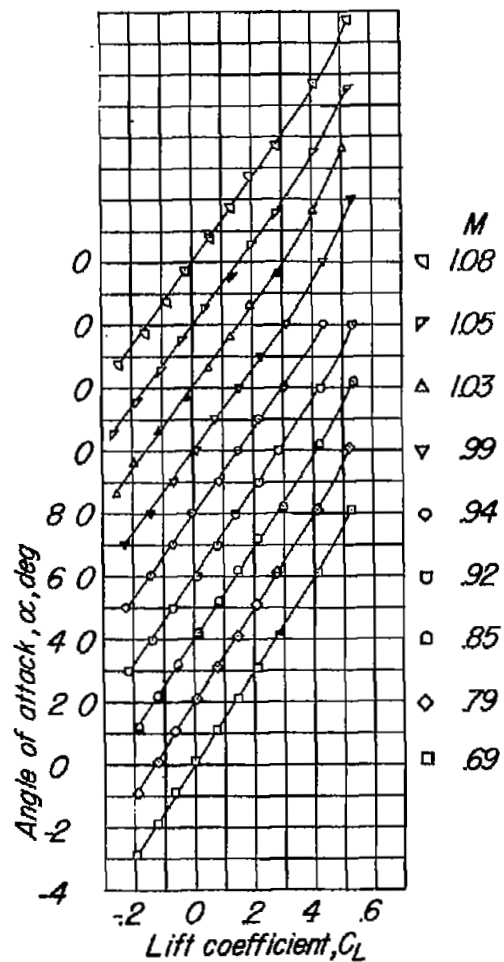
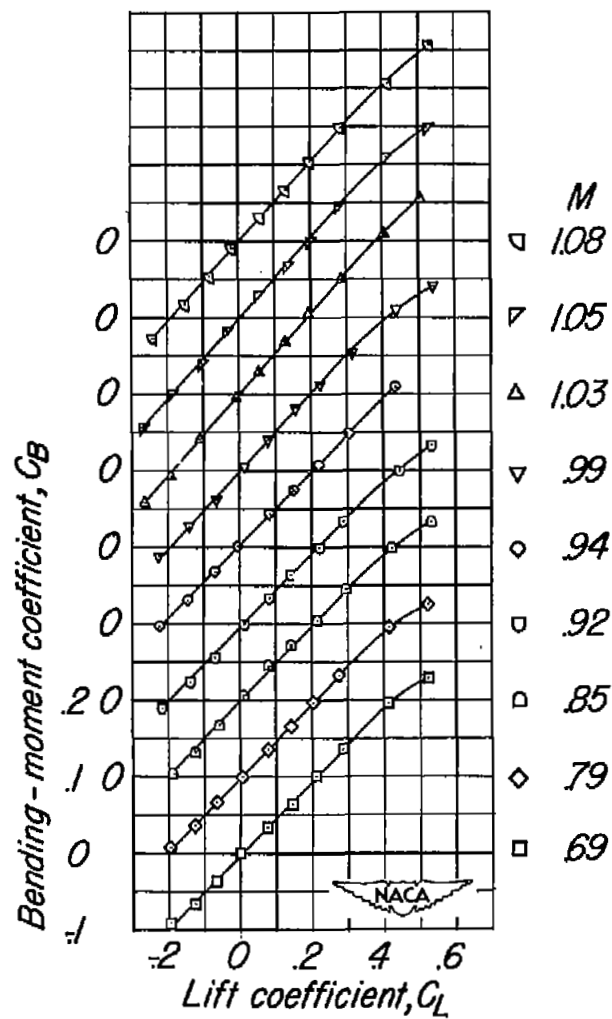
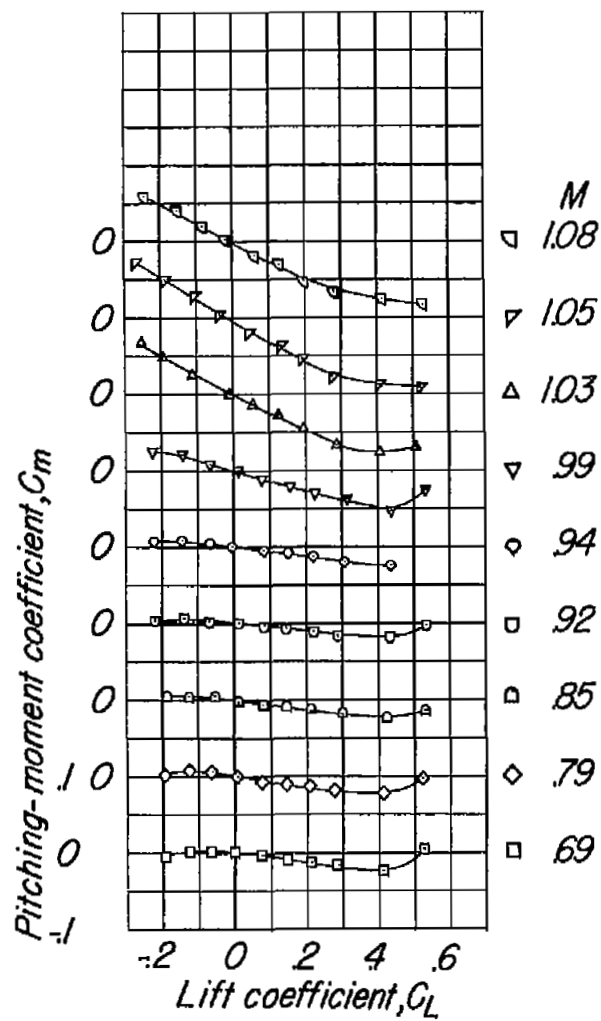


Figure 6.- Concluded.



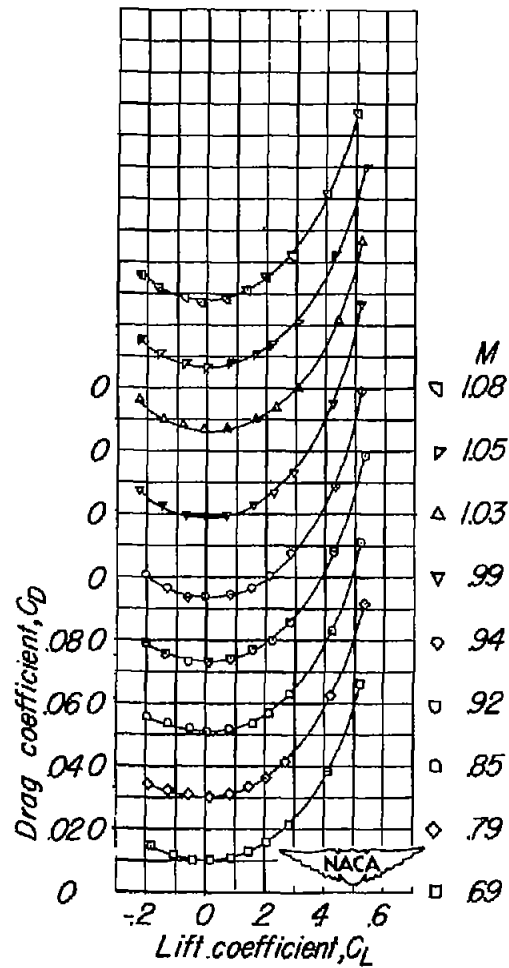
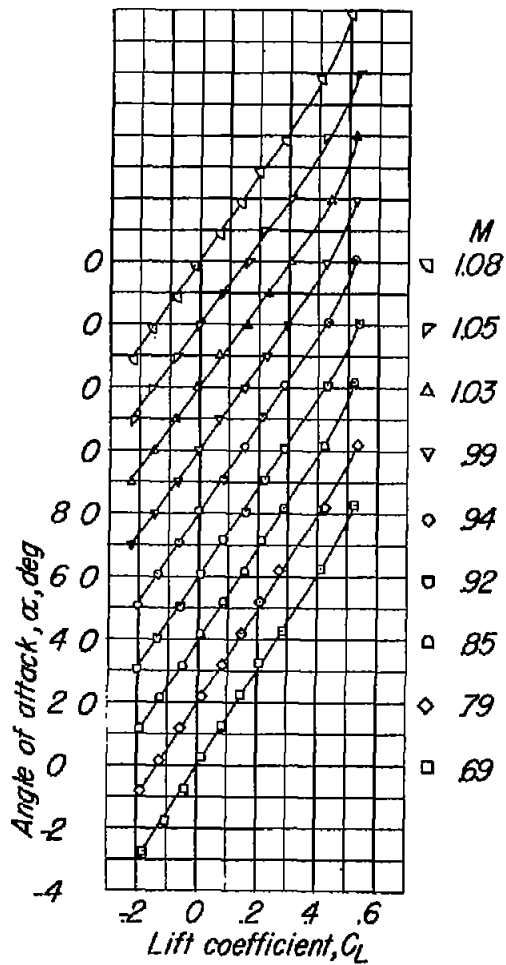
(a) $\frac{y}{b/2} = 0.20.$

Figure 7.- Aerodynamic characteristics of the semispan wing with the nacelle in the symmetrical vertical position.



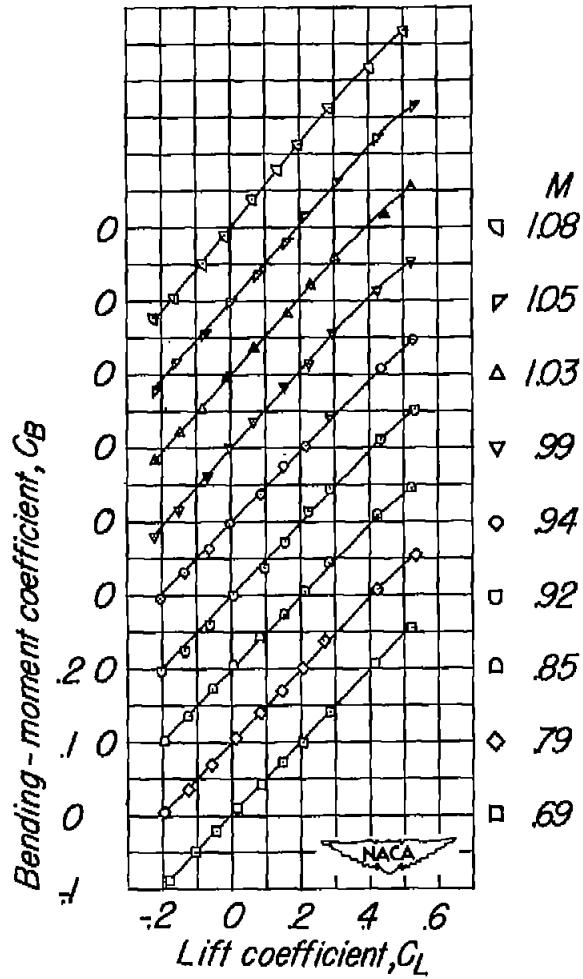
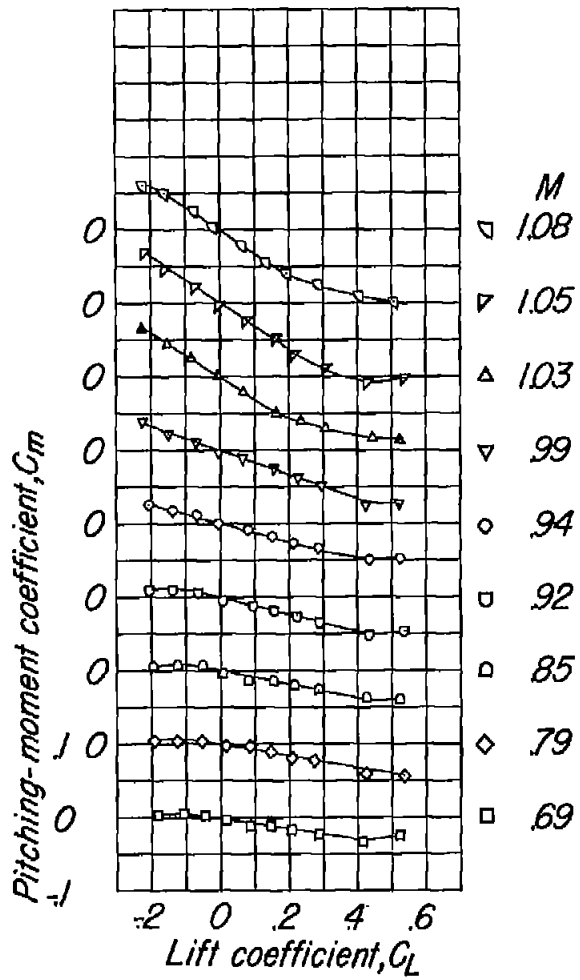
(a) Concluded.

Figure 7.- Continued.



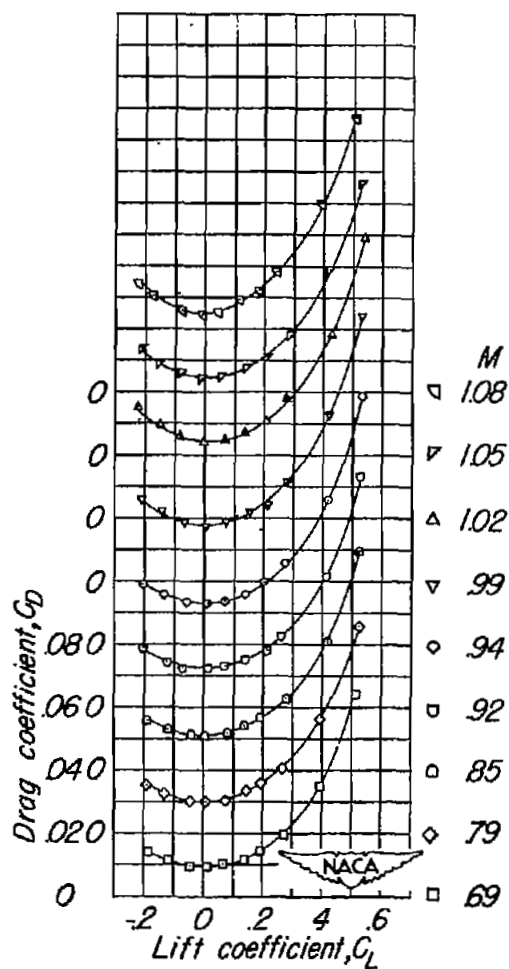
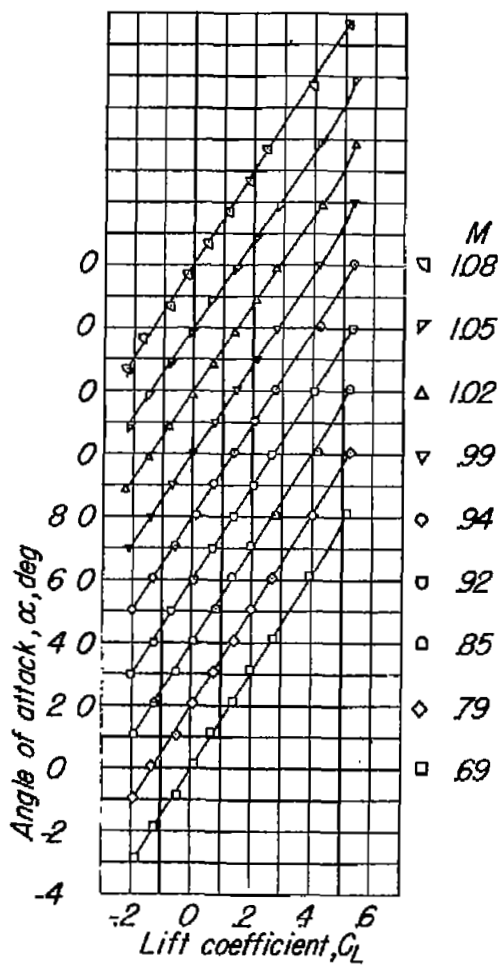
$$(b) \frac{y}{b/2} = 0.46.$$

Figure 7.- Continued.



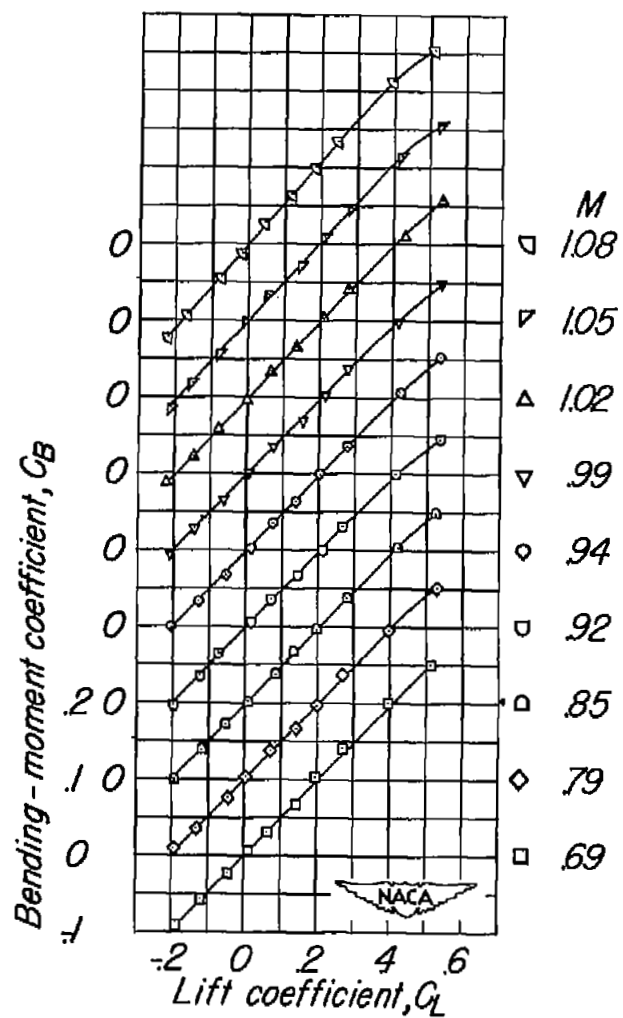
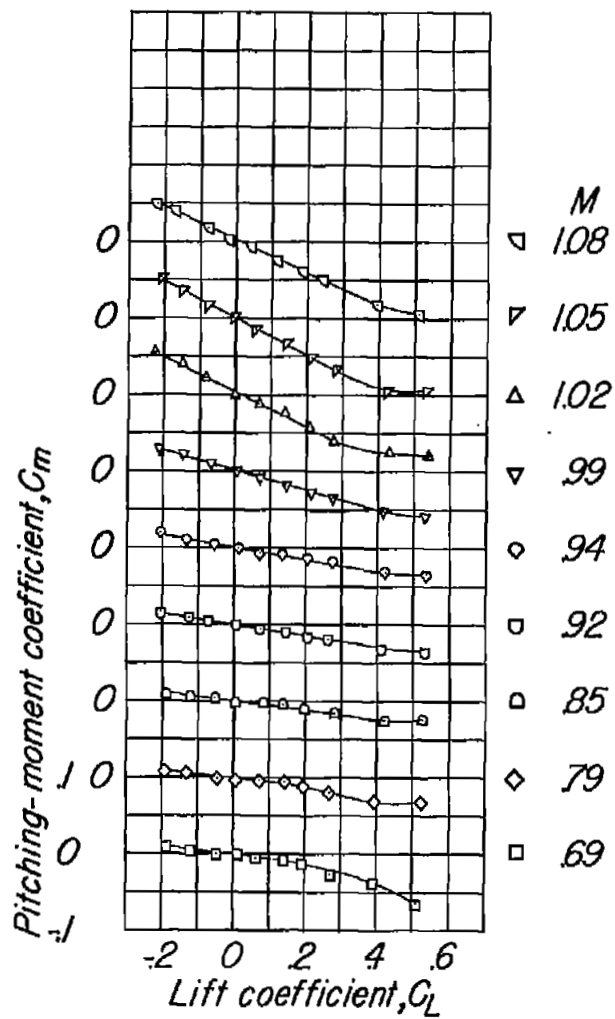
(b) Concluded.

Figure 7.- Continued.



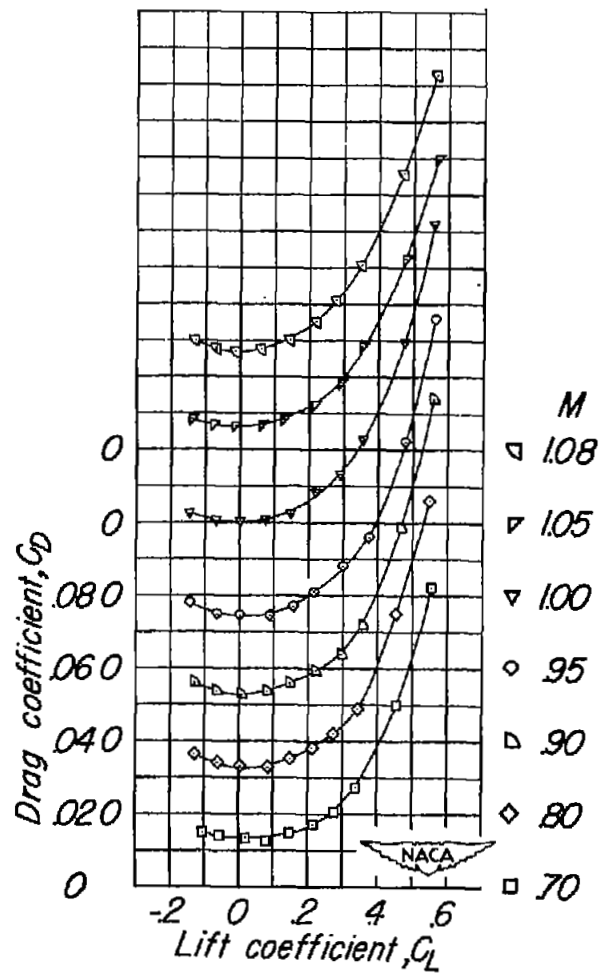
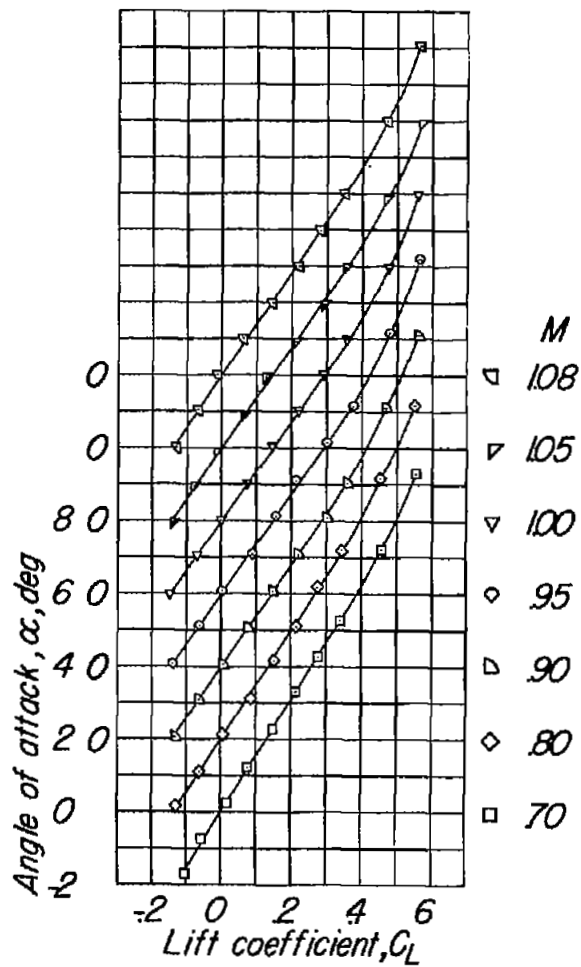
(c) $\frac{y}{b/2} = 0.70.$

Figure 7.- Continued.



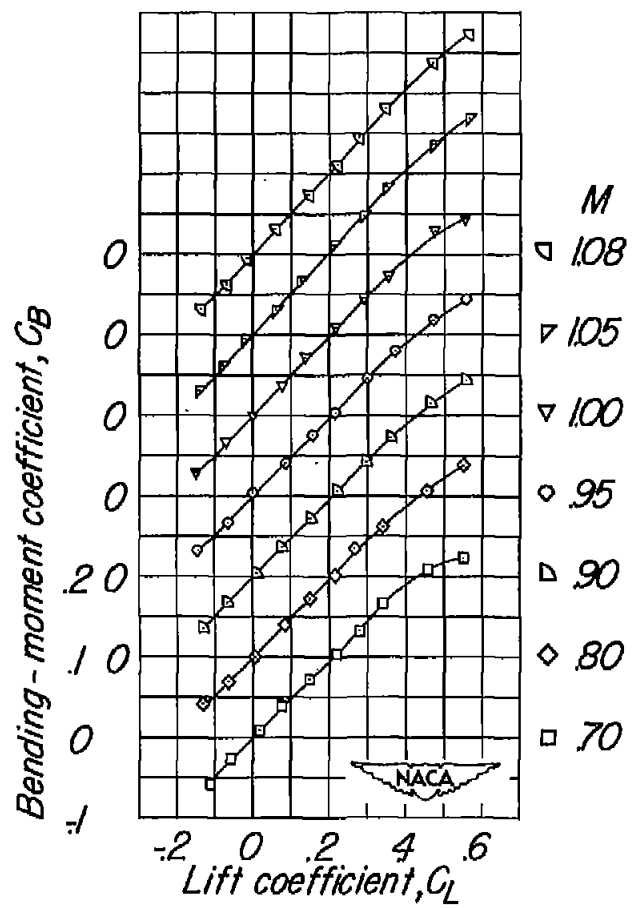
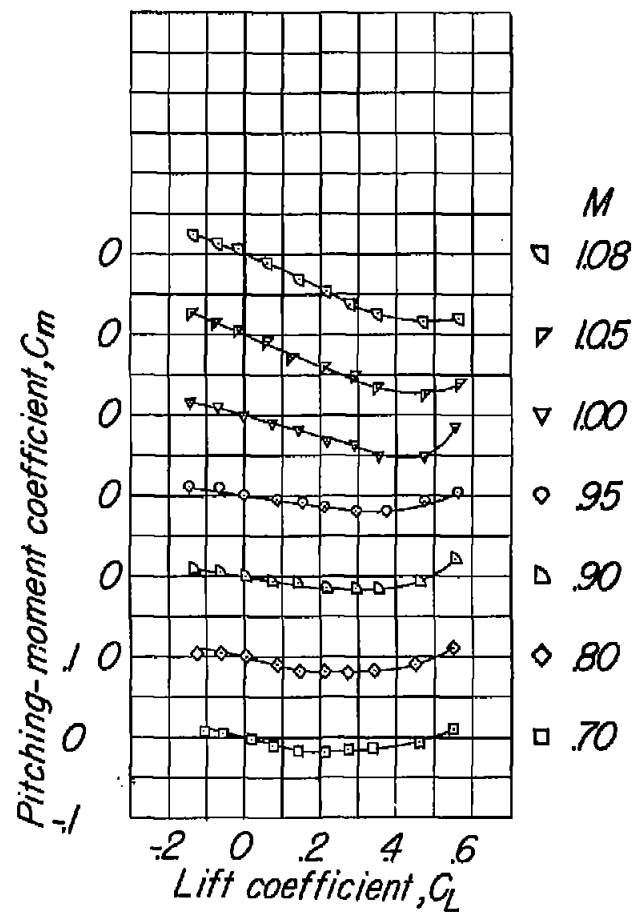
(c) Concluded.

Figure 7.- Continued.



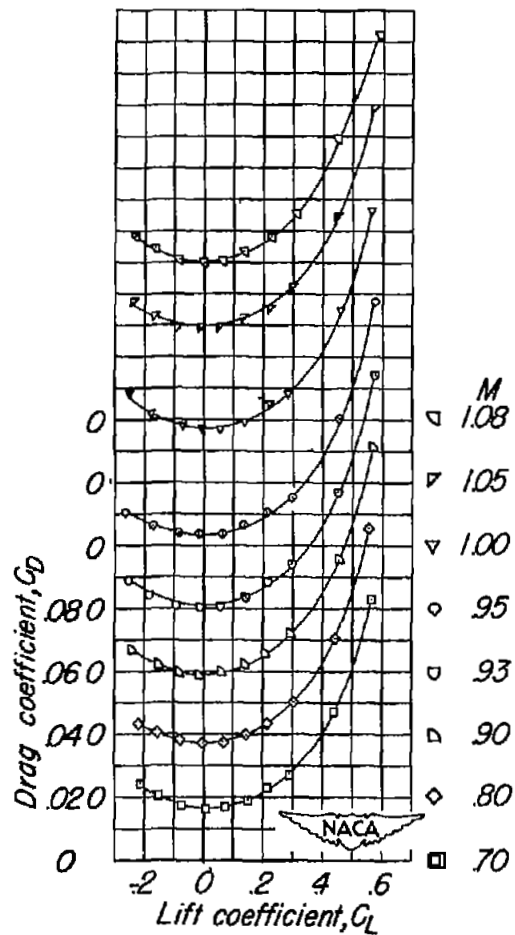
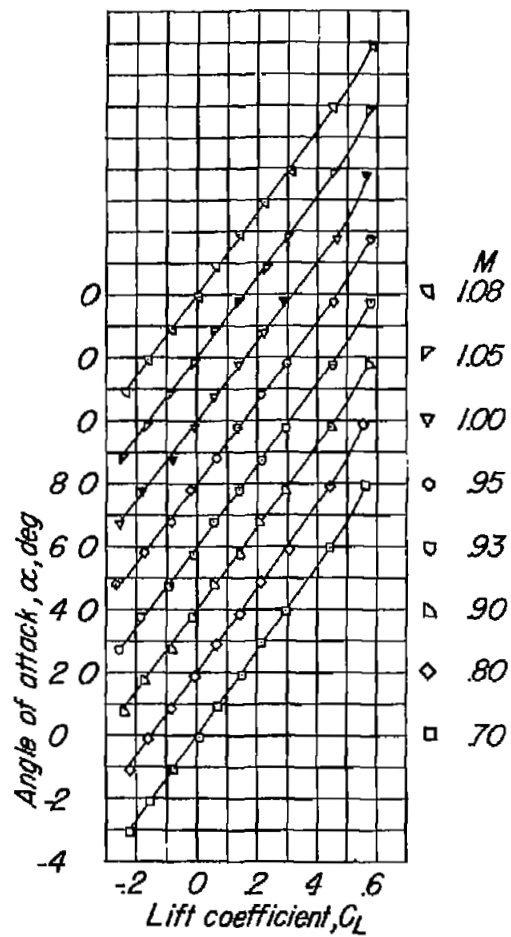
(a) $\frac{y}{b/2} = 0.96.$

Figure 7.- Continued.



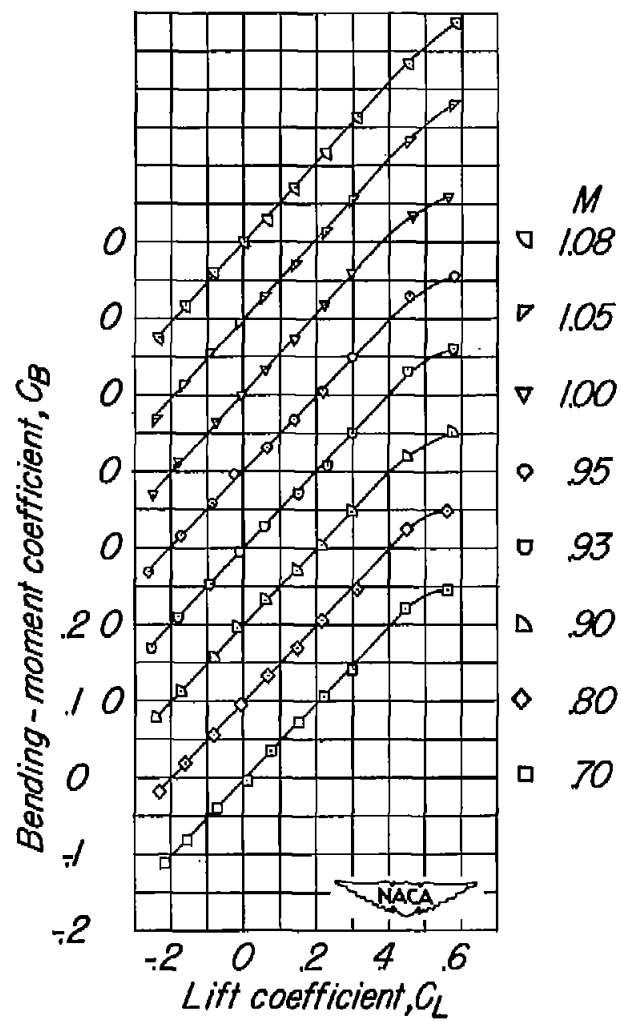
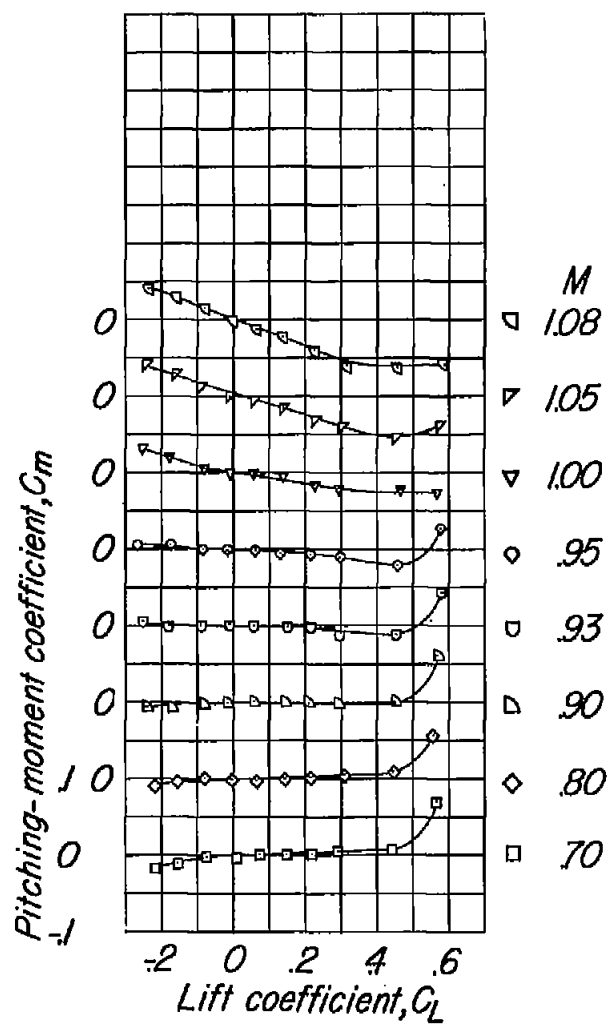
(d) Concluded.

Figure 7.- Concluded.



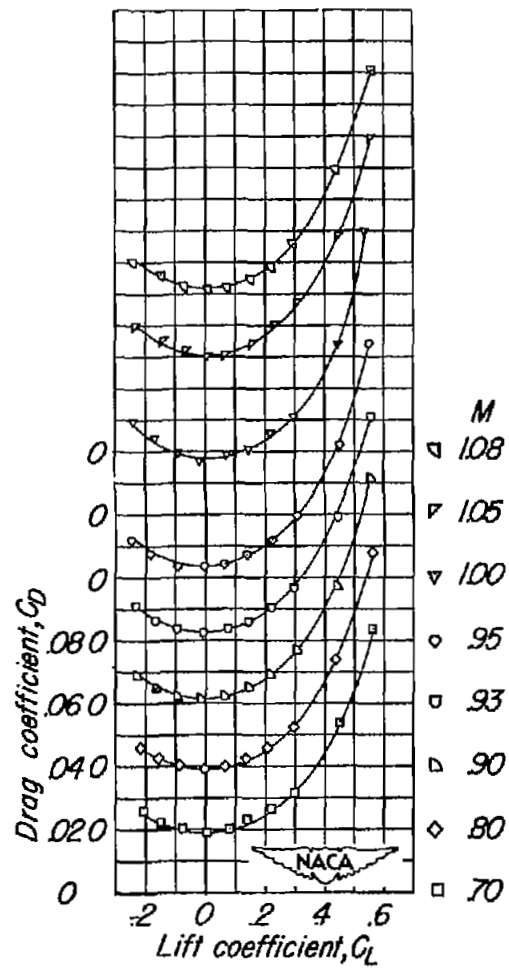
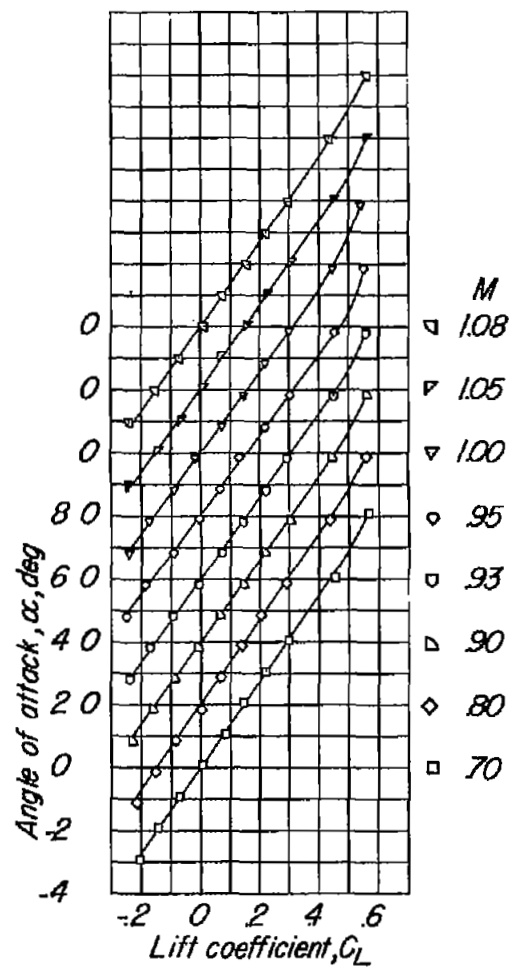
(a) $\frac{y}{b/2} = 0.20.$

Figure 8.- Aerodynamic characteristics of the semispan wing and fuselage combination with the nacelle in the symmetrical position.



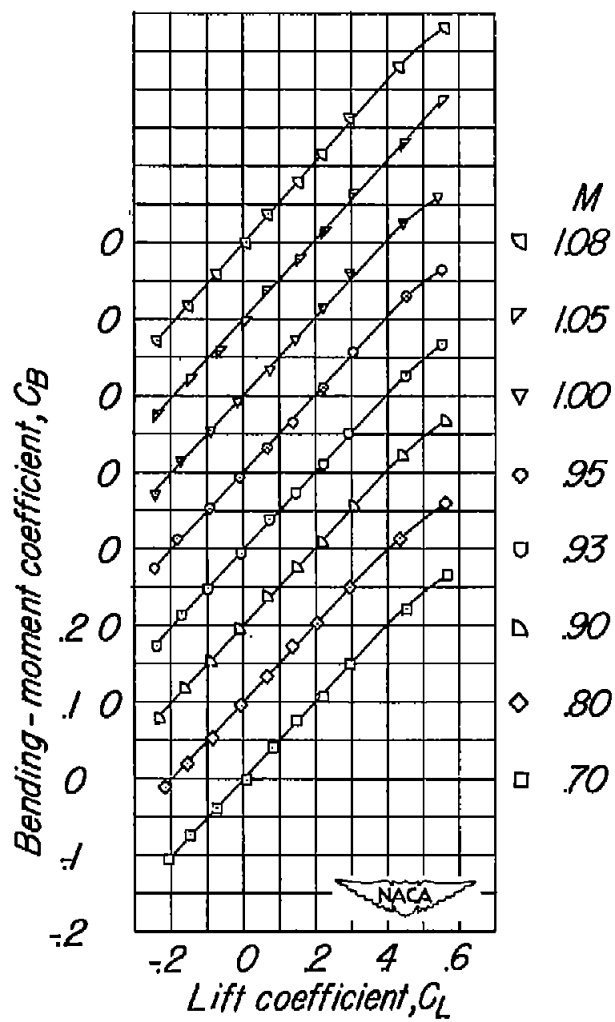
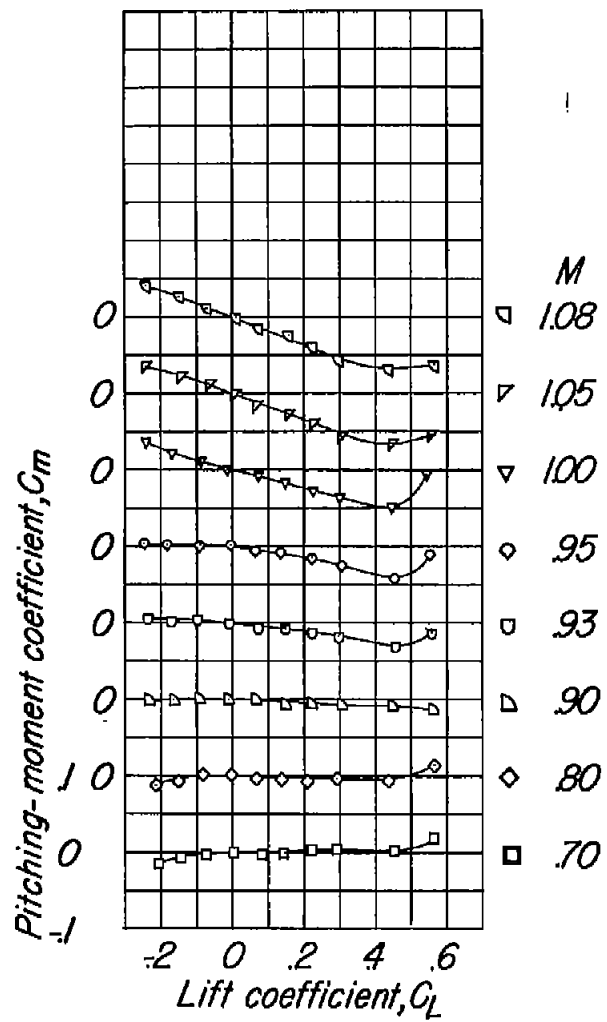
(a) Concluded.

Figure 8.- Continued.



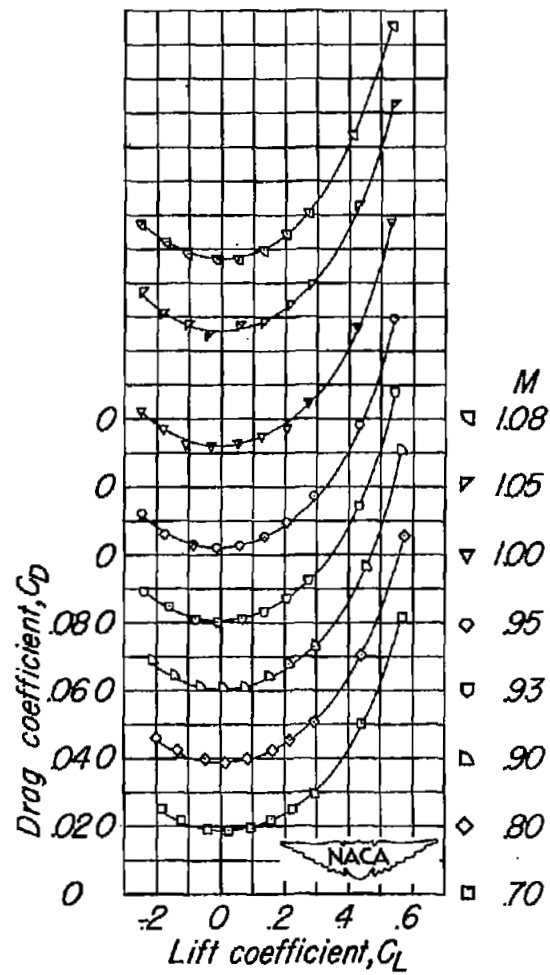
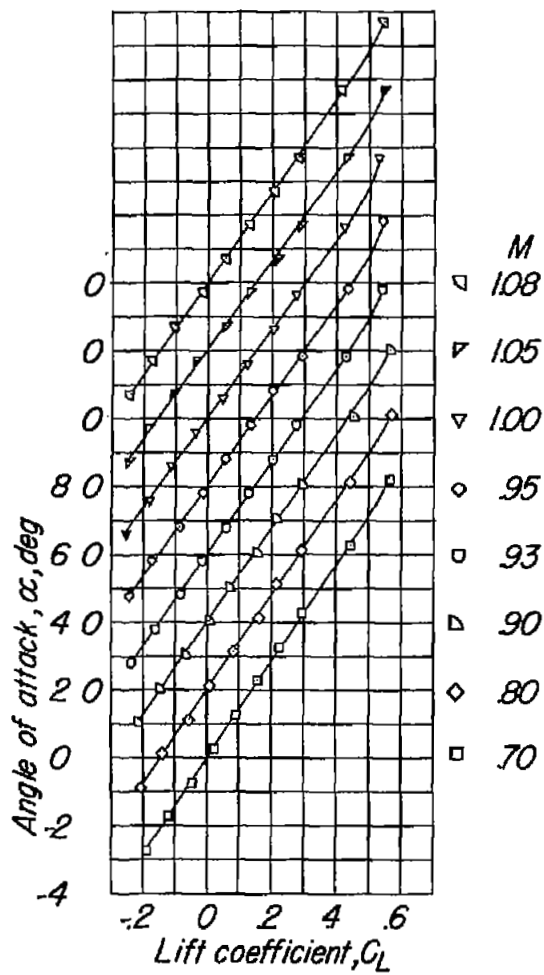
(b) $\frac{y}{b/2} = 0.46.$

Figure 8.- Continued.



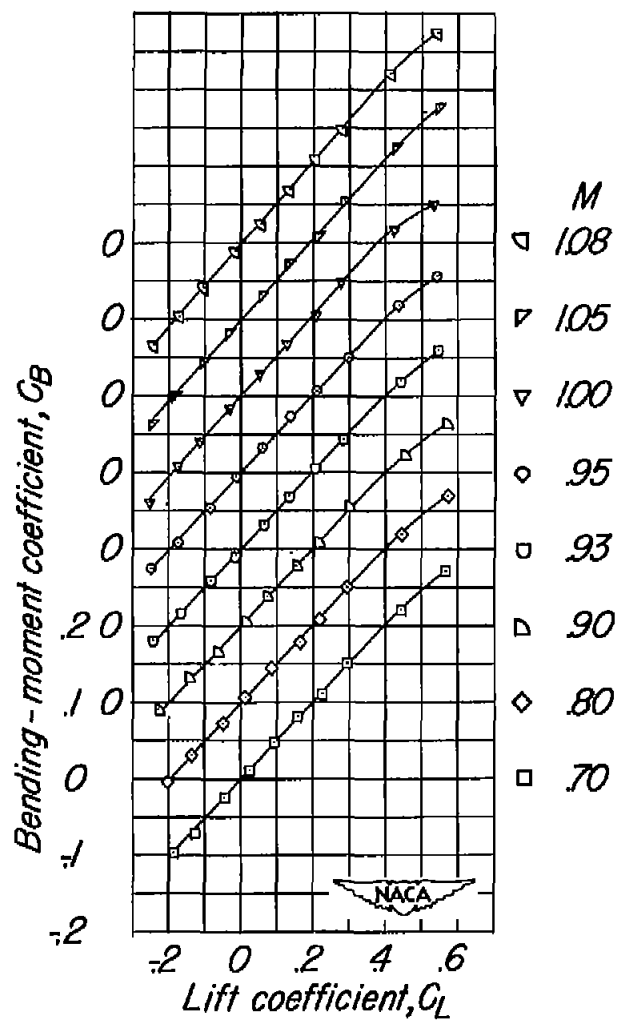
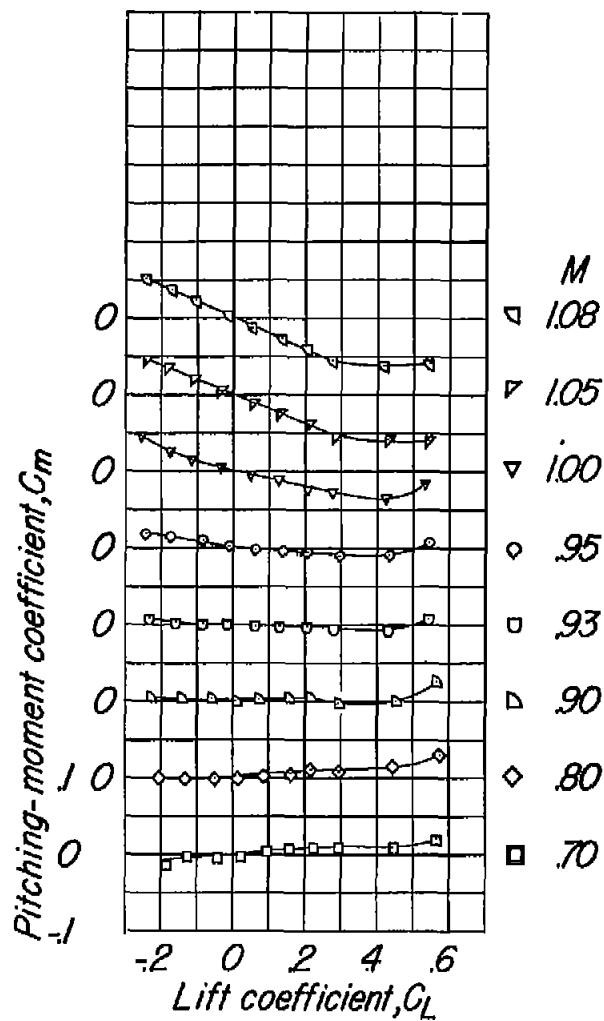
(b) Concluded.

Figure 8.- Continued.



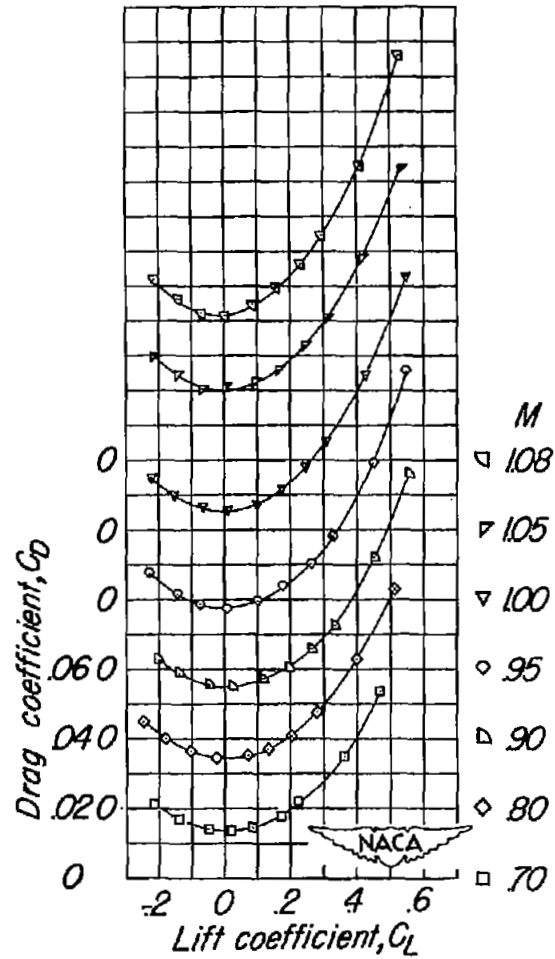
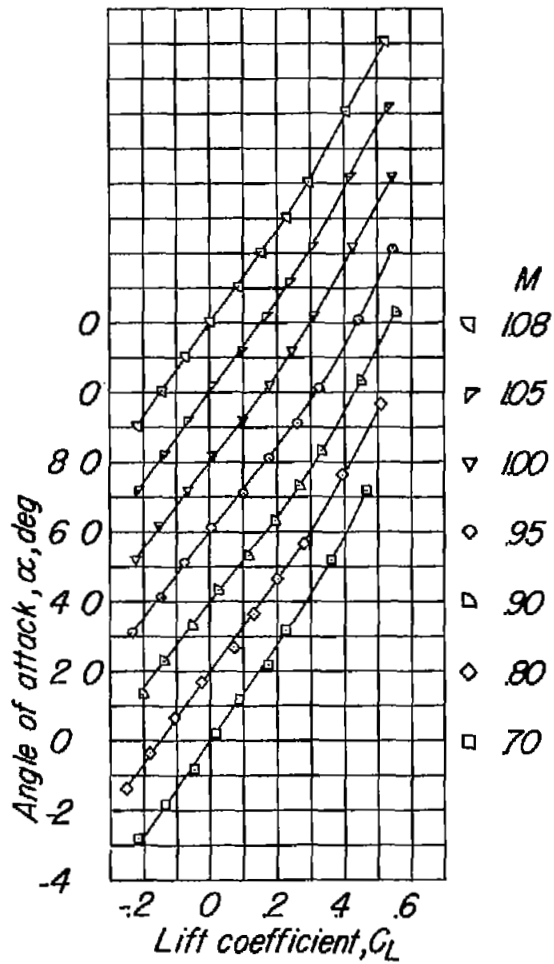
$$(c) \frac{y}{b/2} = 0.70.$$

Figure 8.- Continued.



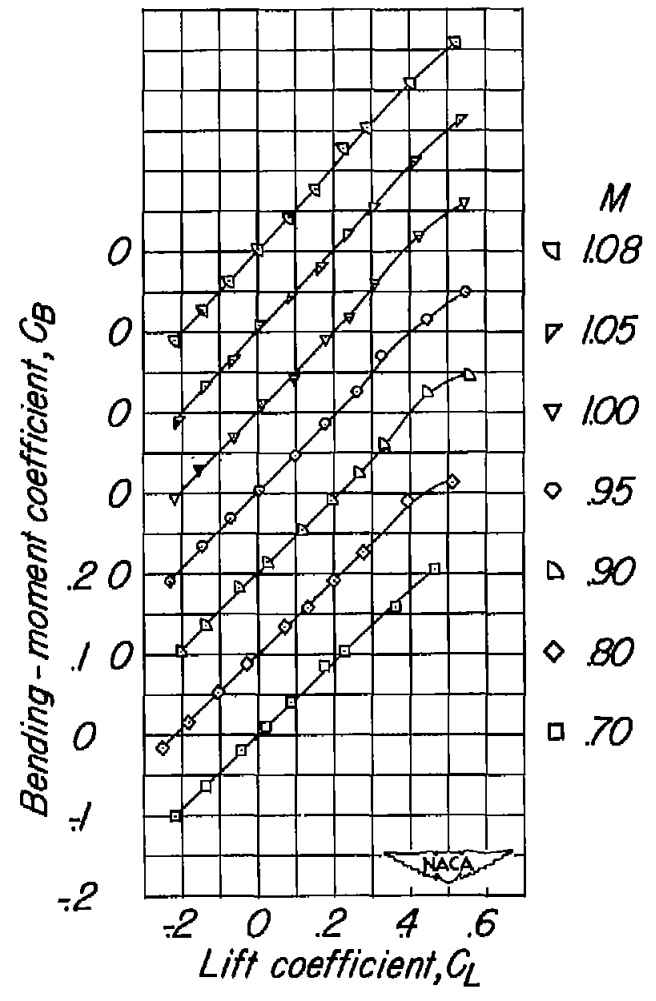
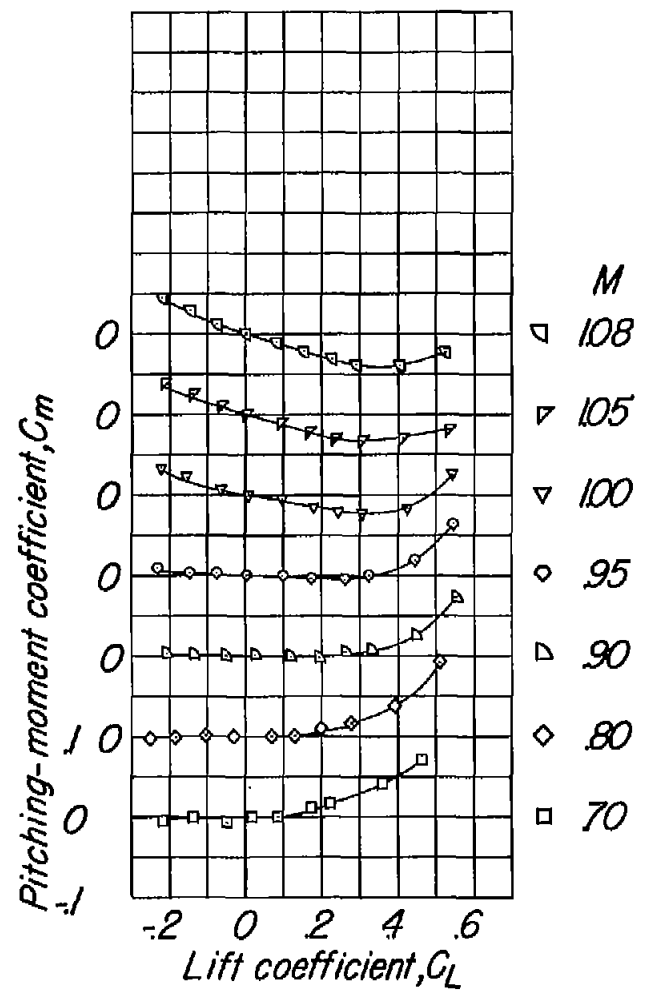
(c) Concluded.

Figure 8.- Continued.



(a) $\frac{y}{b/2} = 0.96$.

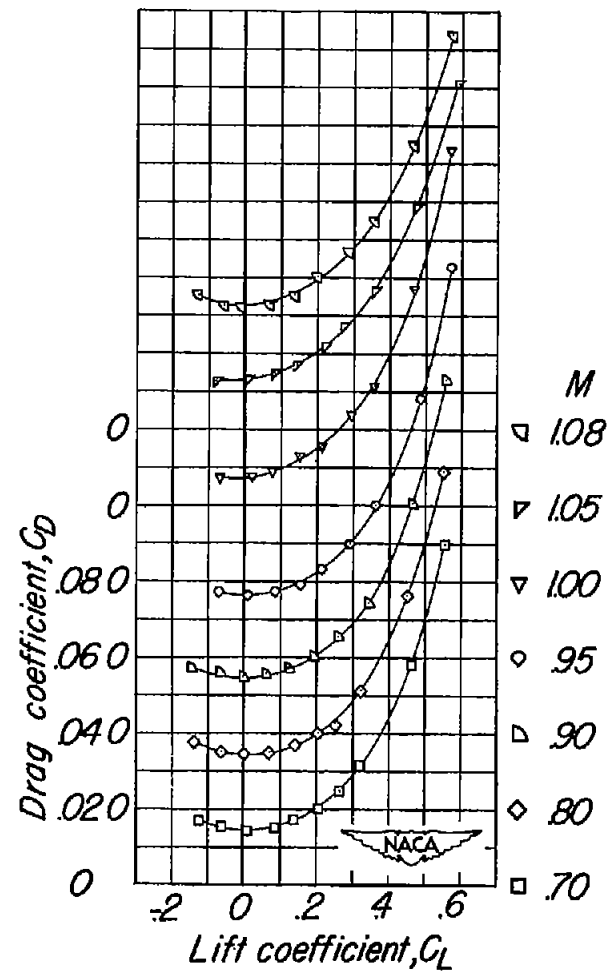
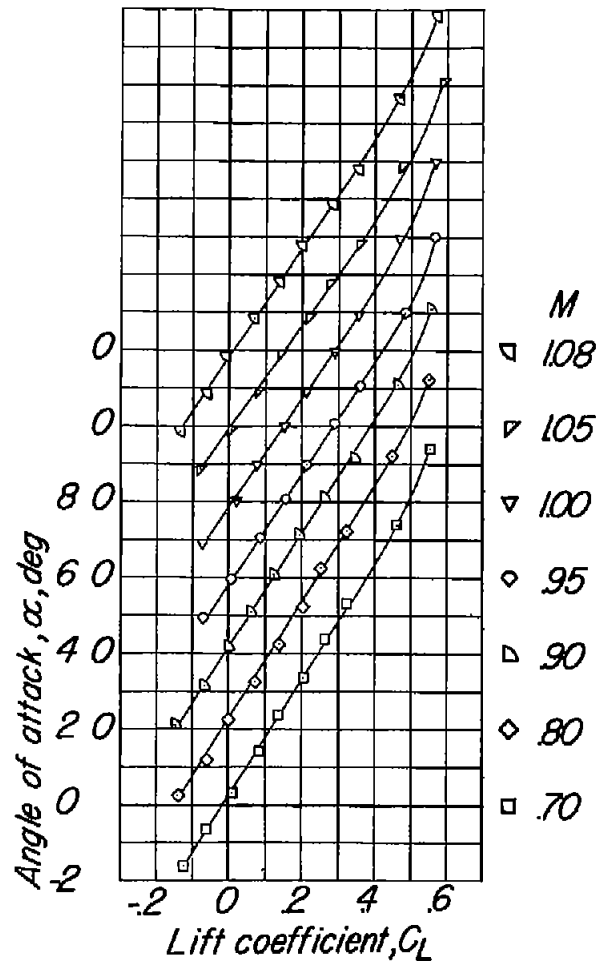
Figure 8.- Continued.



(d) Concluded.

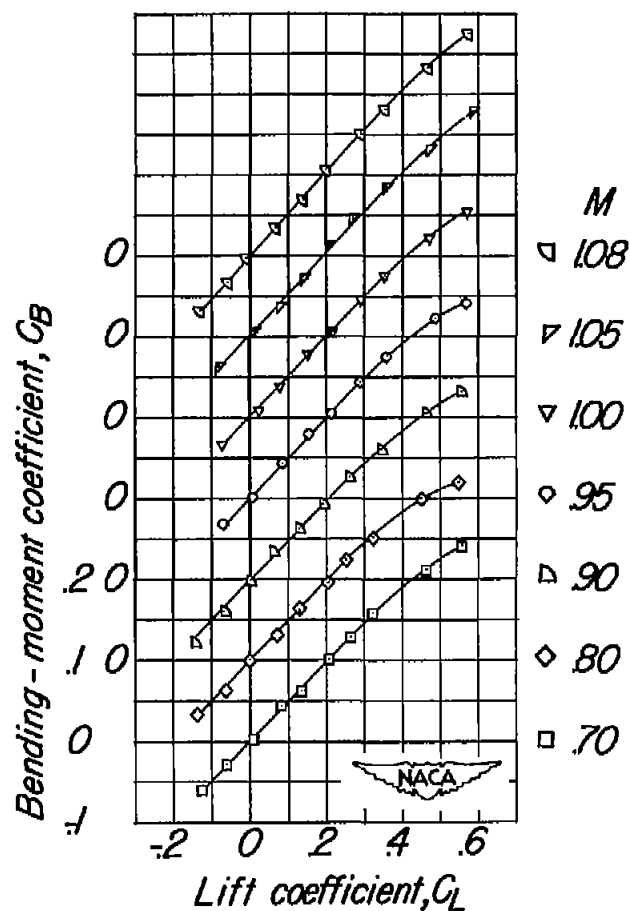
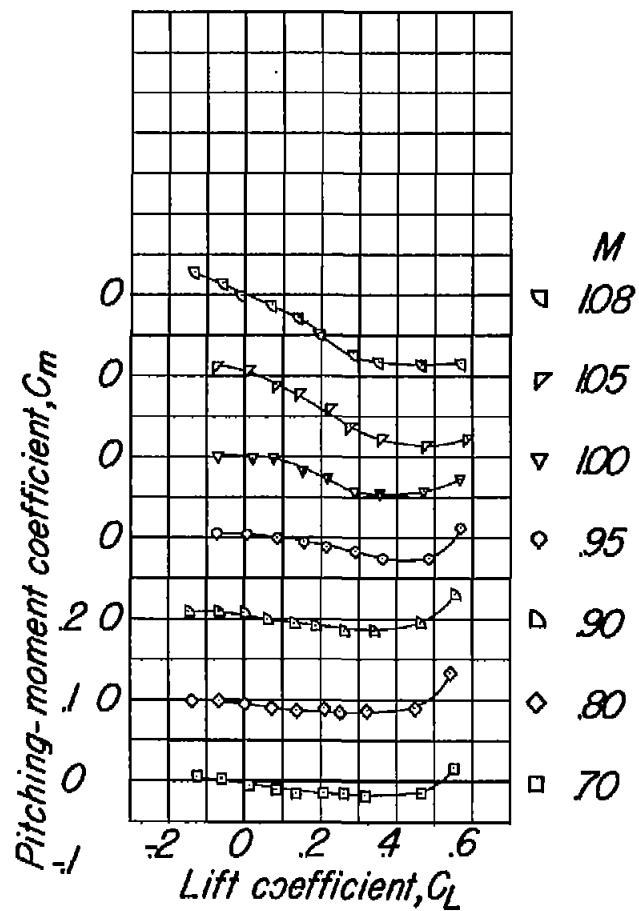
Figure 8.- Concluded.

CONFIDENTIAL



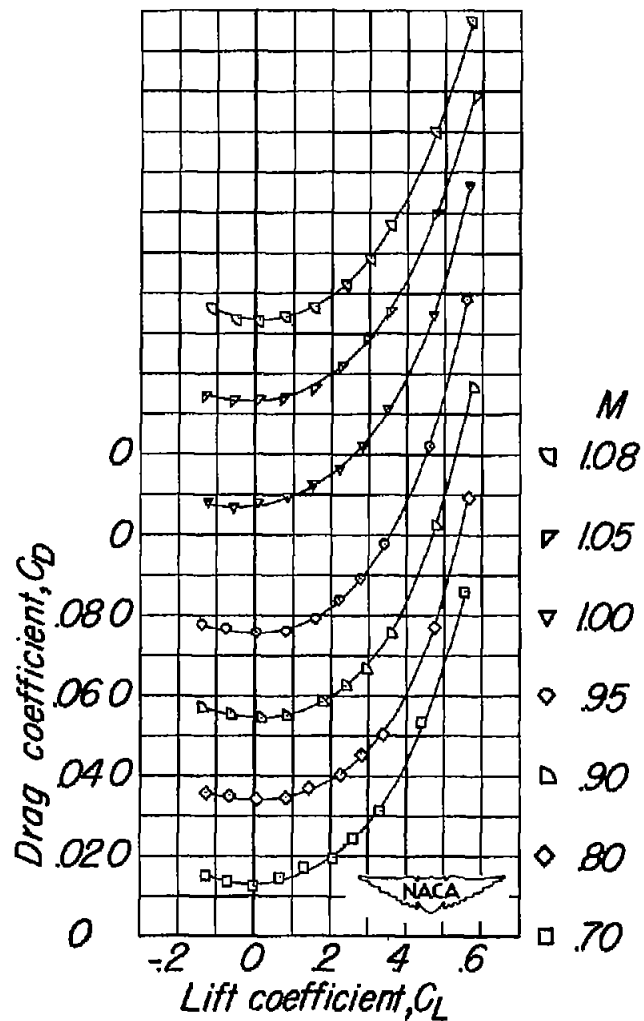
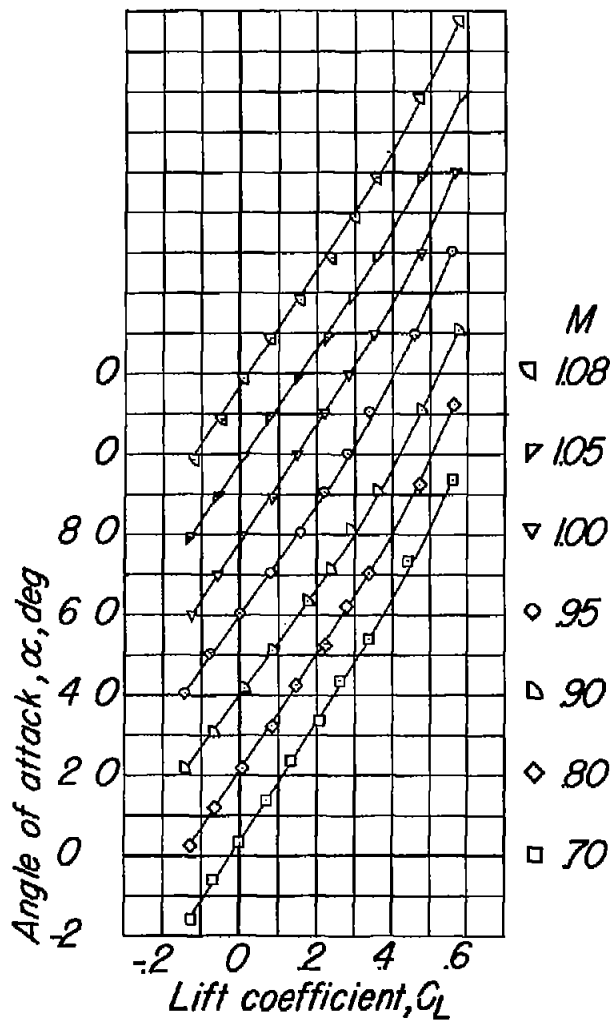
(a) $\frac{y}{b/2} = 0.20$.

Figure 9.- Aerodynamic characteristics of the semispan wing with the nacelle in the underwing position.



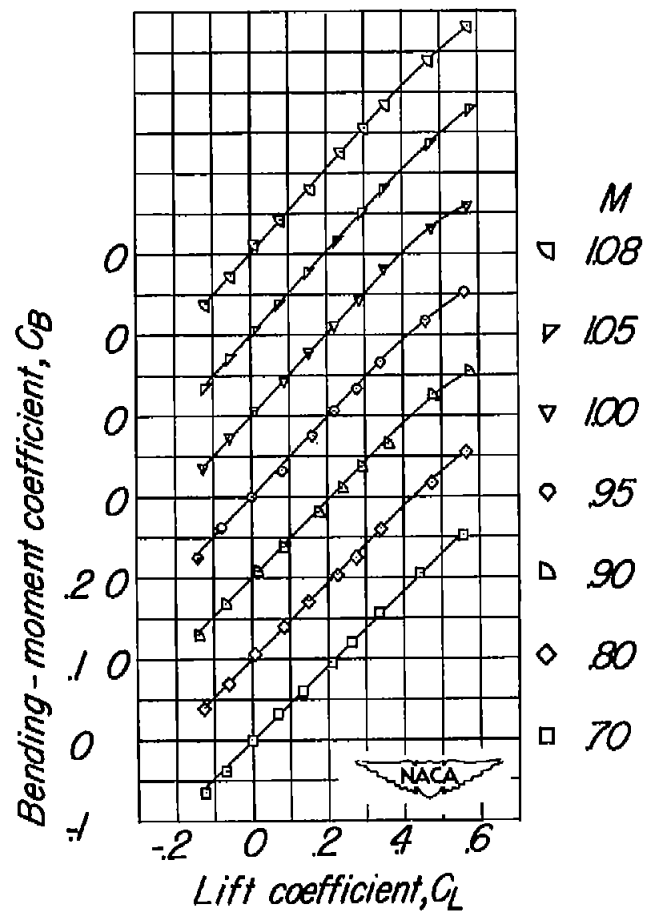
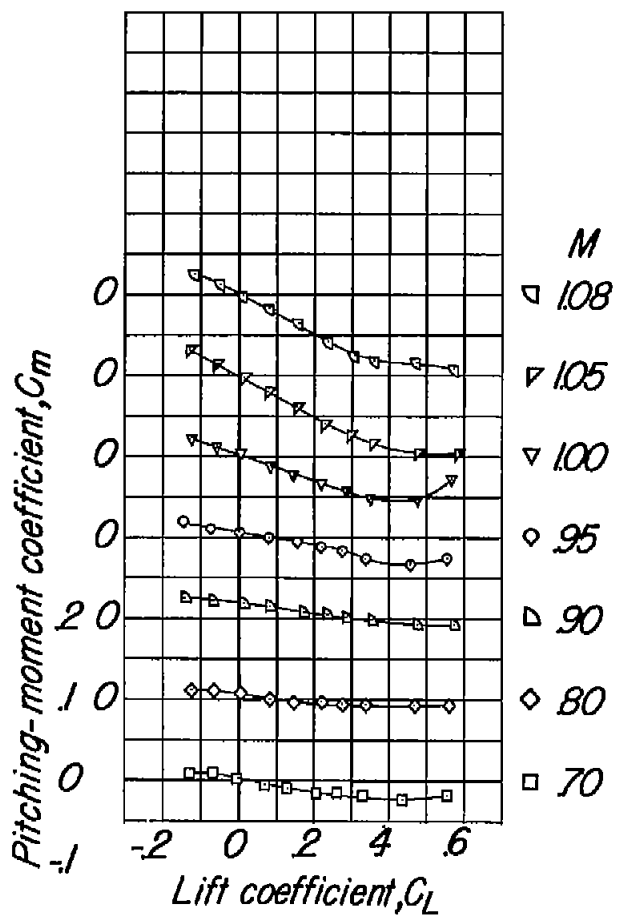
(a) Concluded.

Figure 9.- Continued.



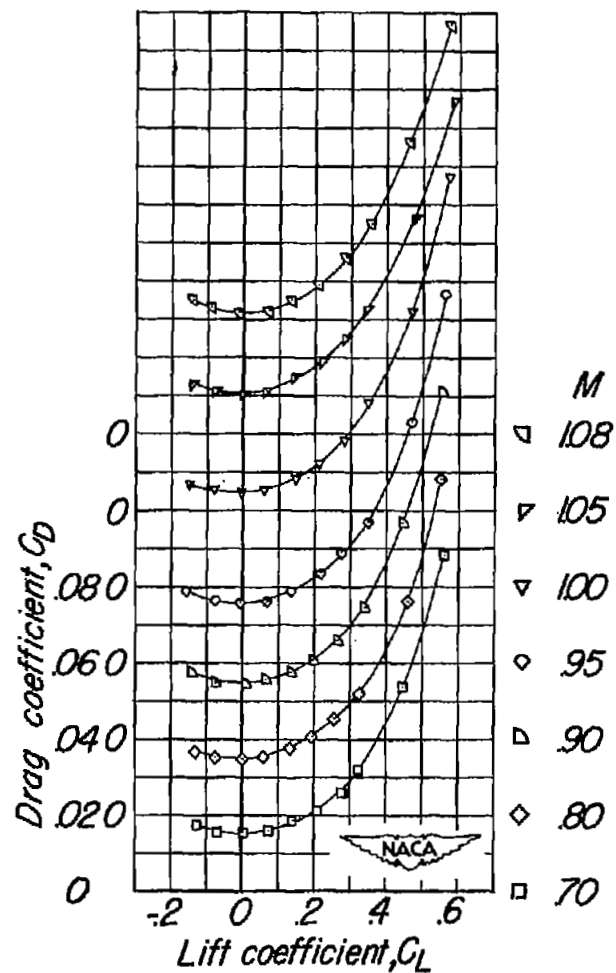
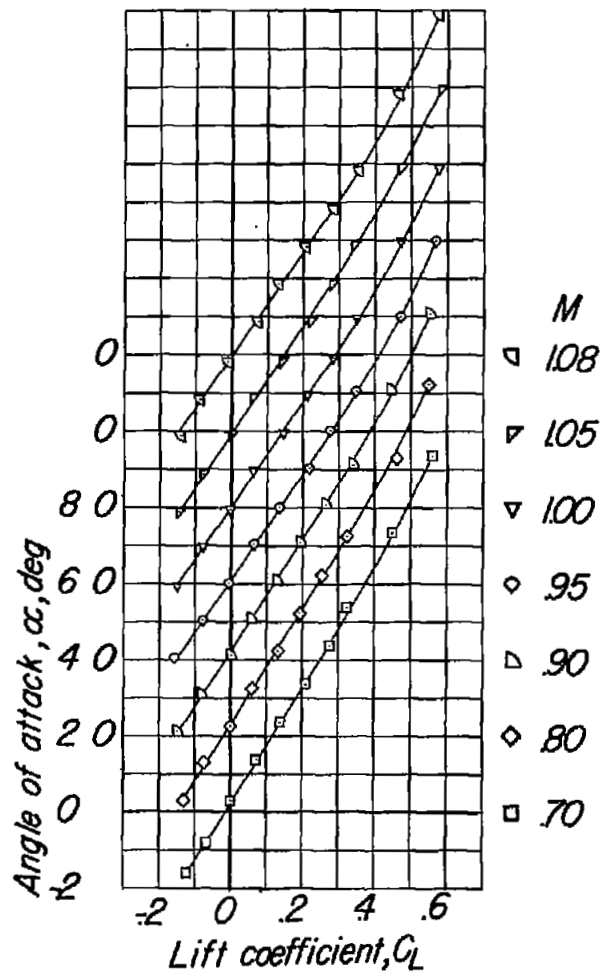
(b) $\frac{y}{b/2} = 0.46.$

Figure 9.- Continued.



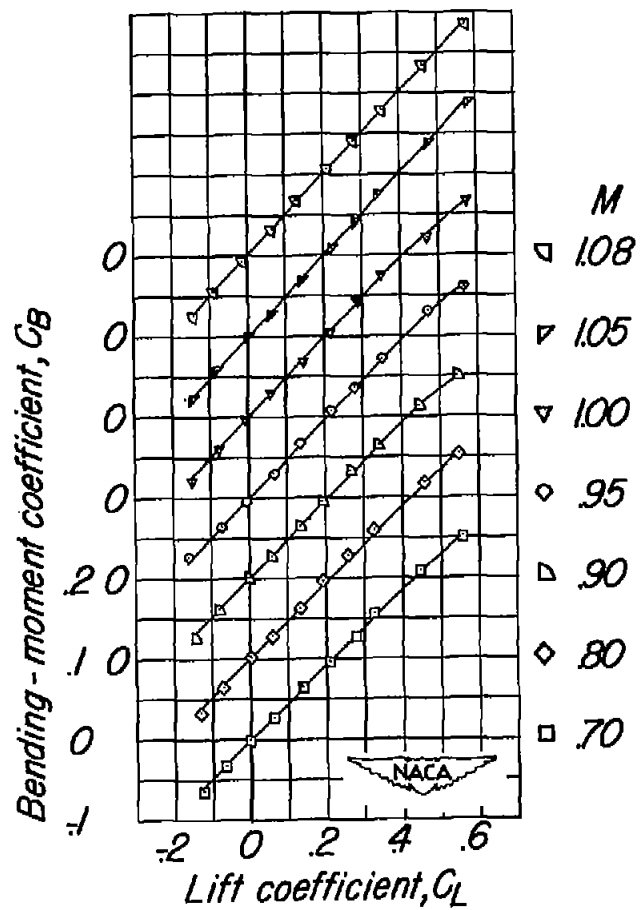
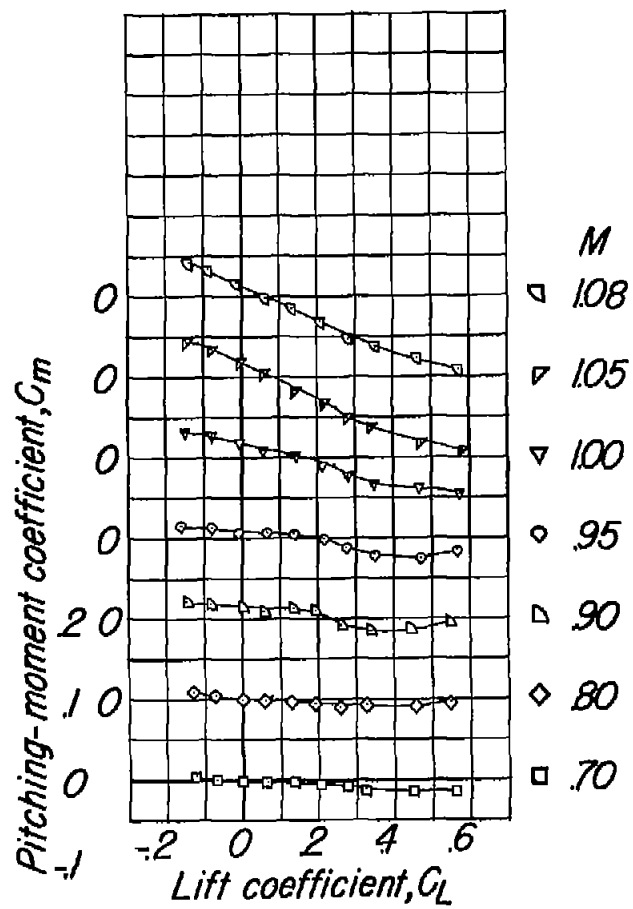
(b) Concluded.

Figure 9.- Continued.



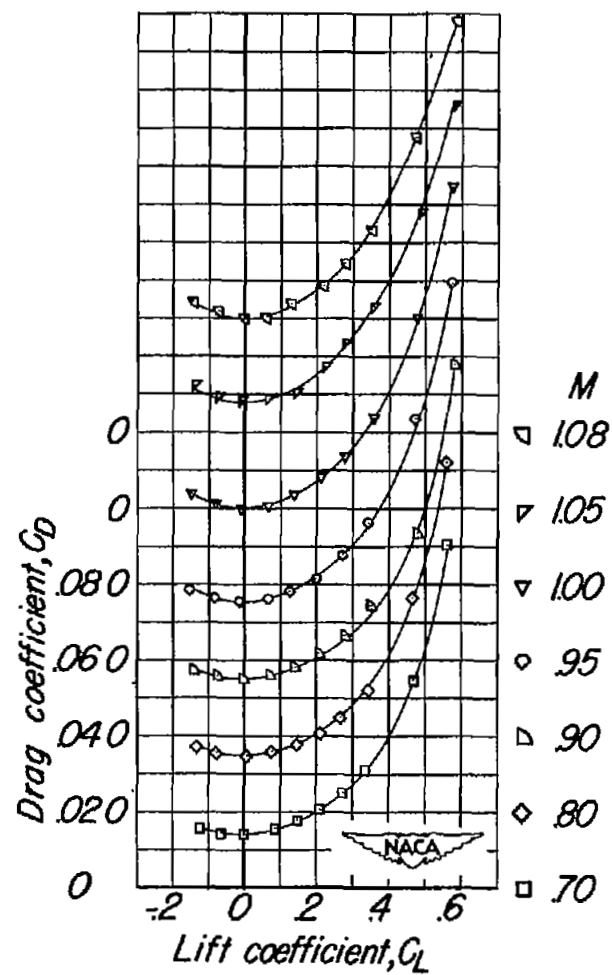
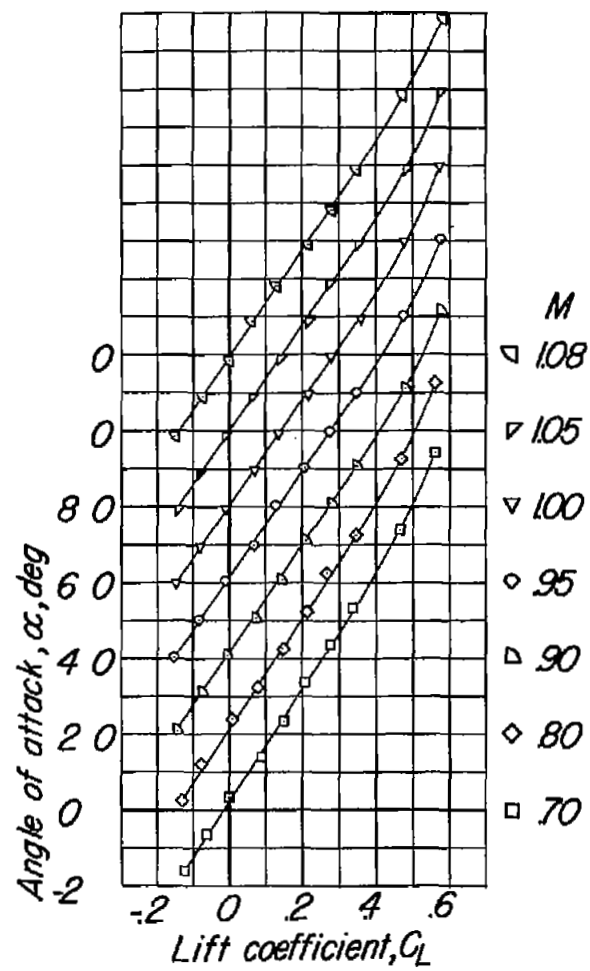
(c) $\frac{y}{b/2} = 0.70.$

Figure 9.- Continued.



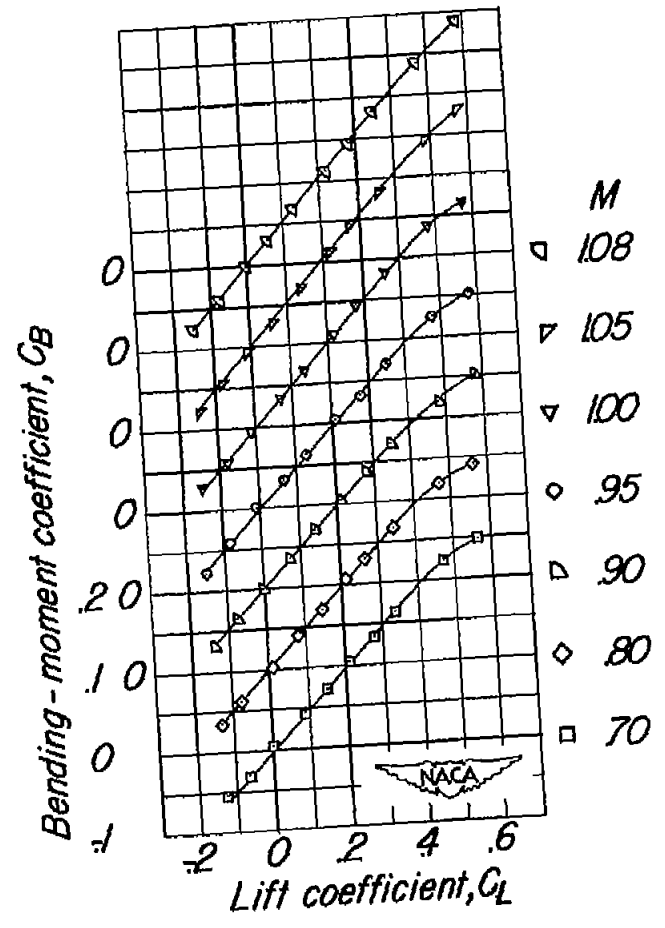
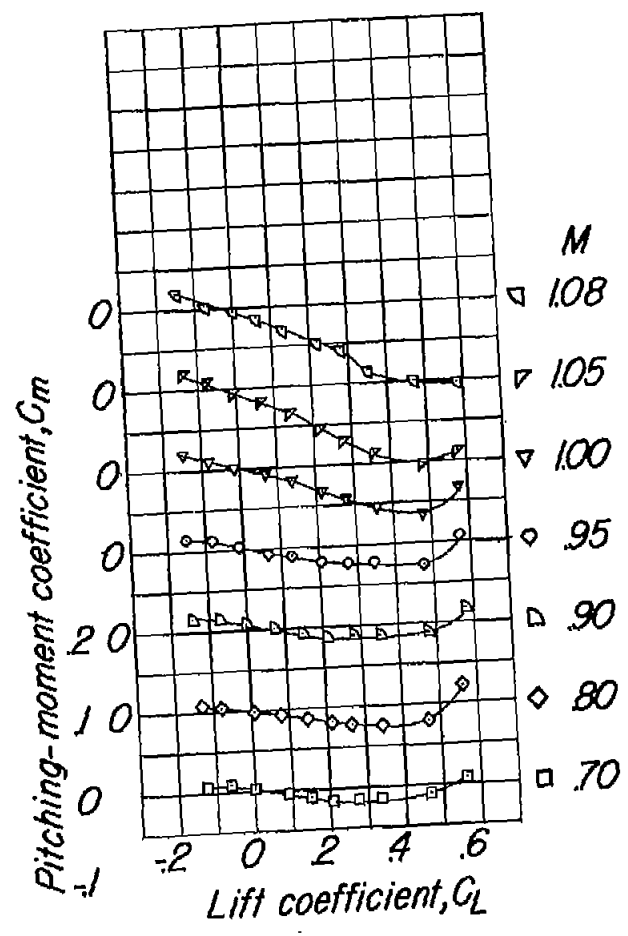
(c) Concluded.

Figure 9.- Continued.



(a) $\frac{y}{b/2} = 0.96.$

Figure 9.- Continued.



(d) Concluded.

Figure 9.- Concluded.

y/b

- Off
- - - 20
- - - 46
- - - 70
- - - 96

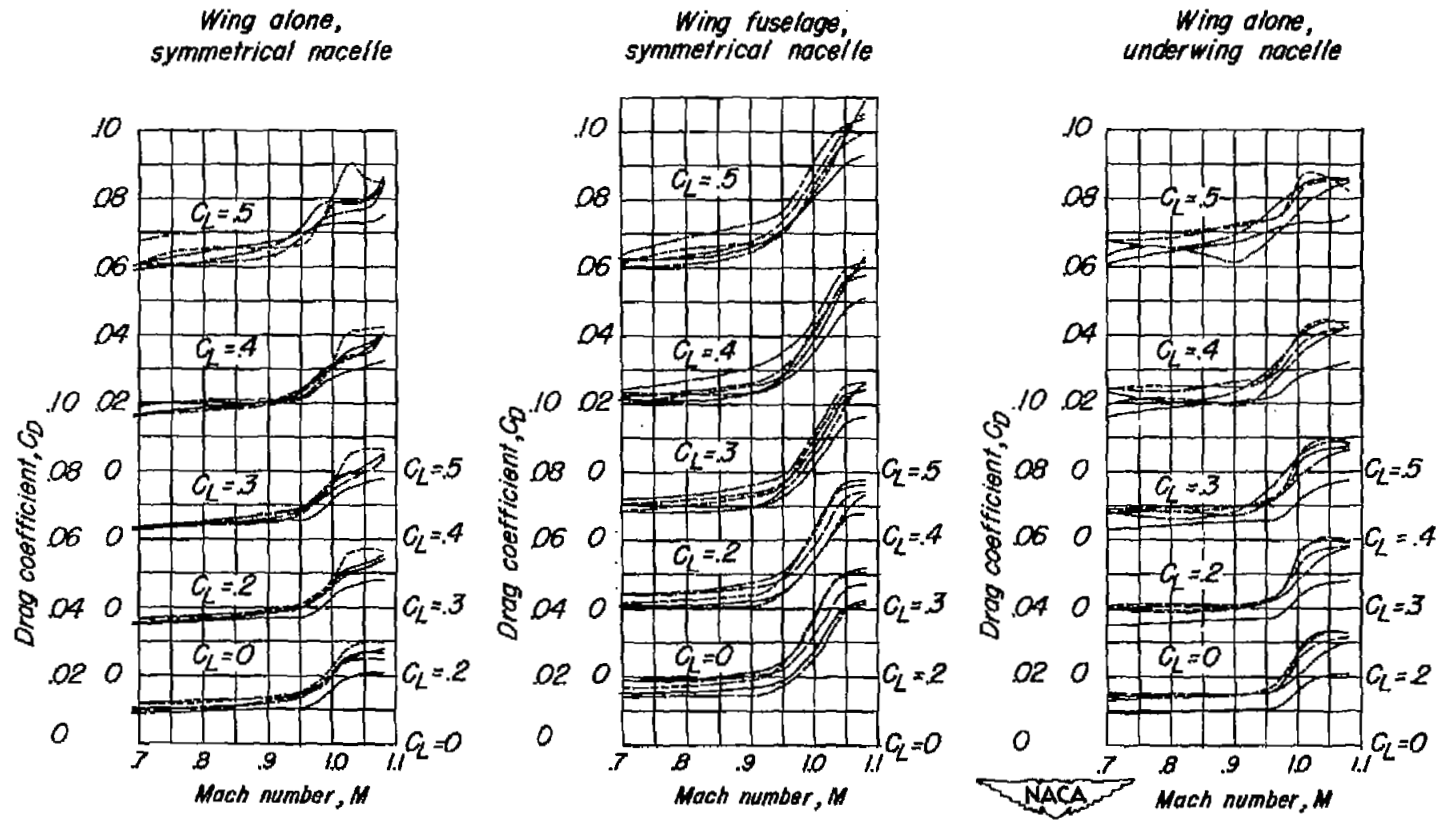


Figure 10.- Variation of drag coefficient with Mach number for the models with and without the nacelle in various chordwise locations.

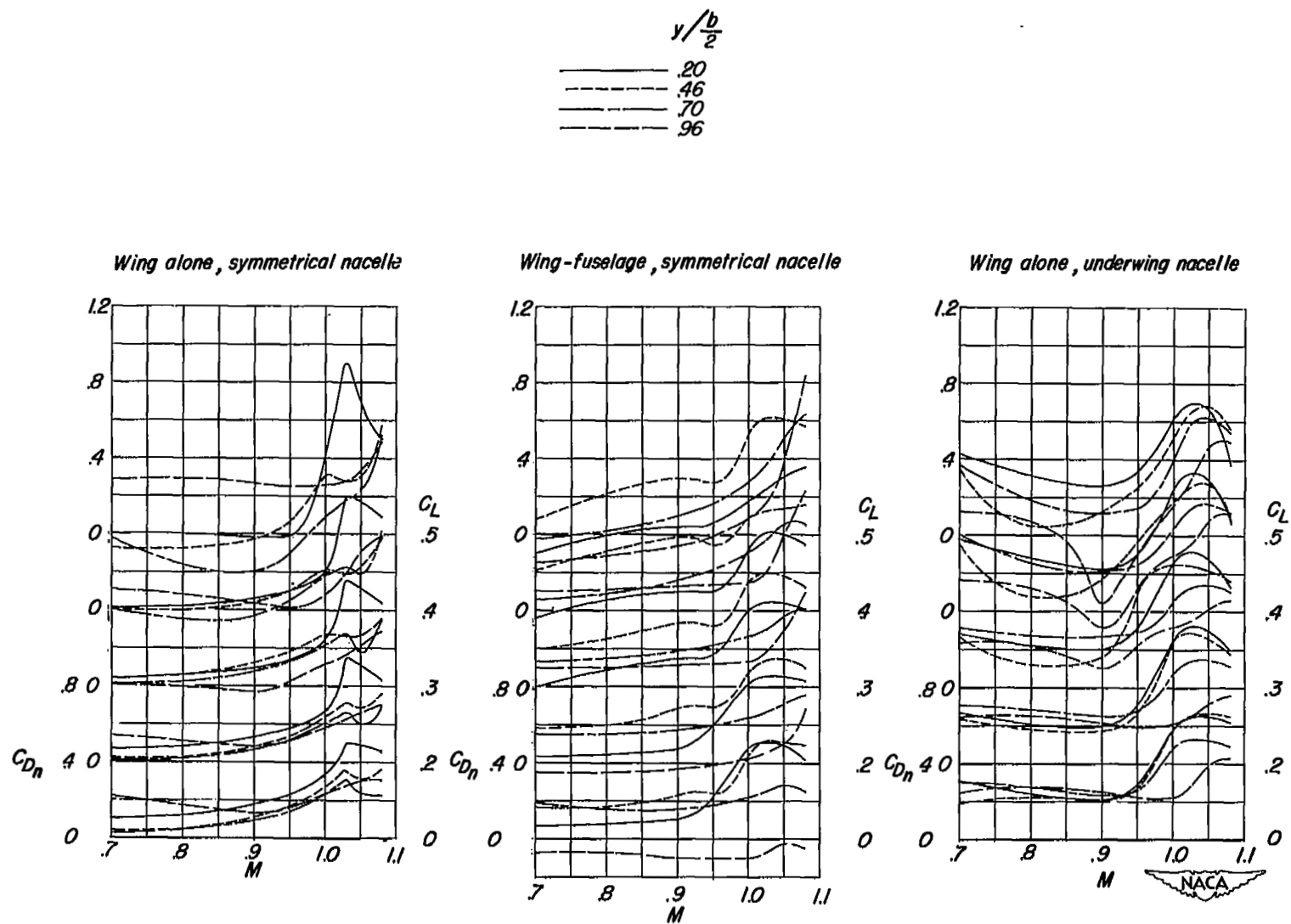


Figure 11.- Variation of nacelle drag coefficient with Mach number.

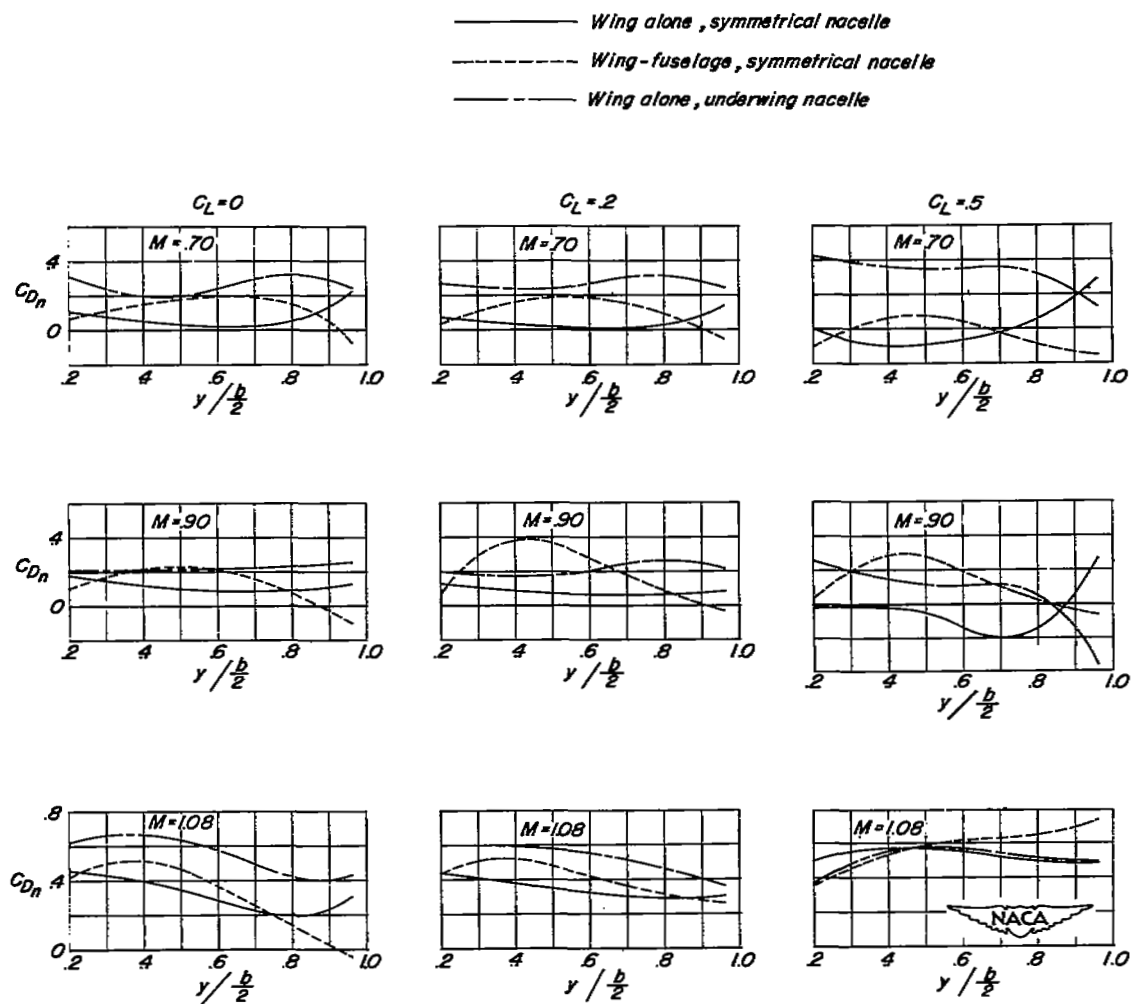
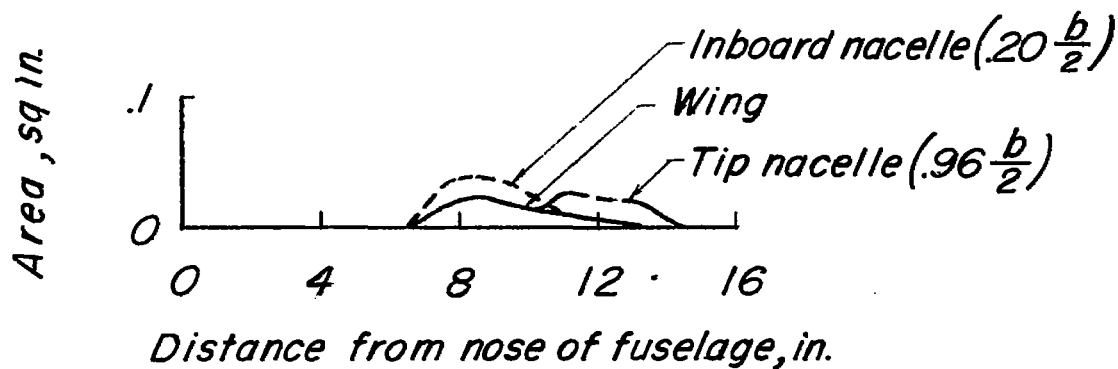
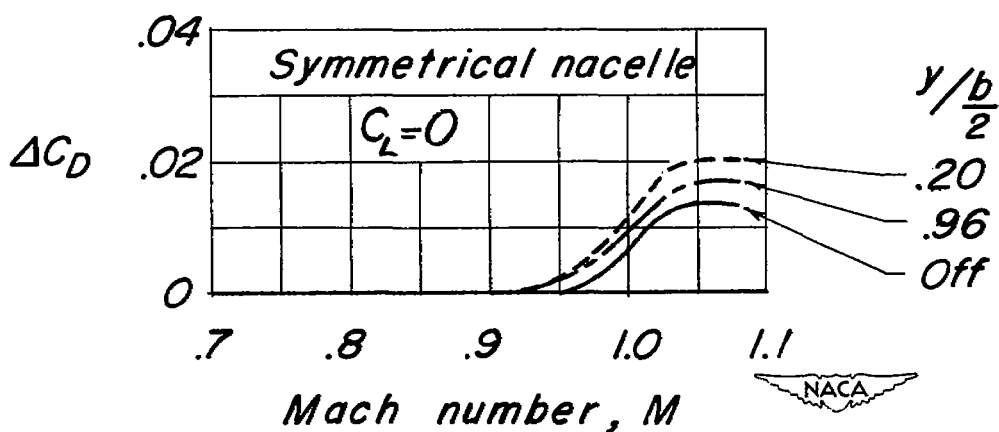
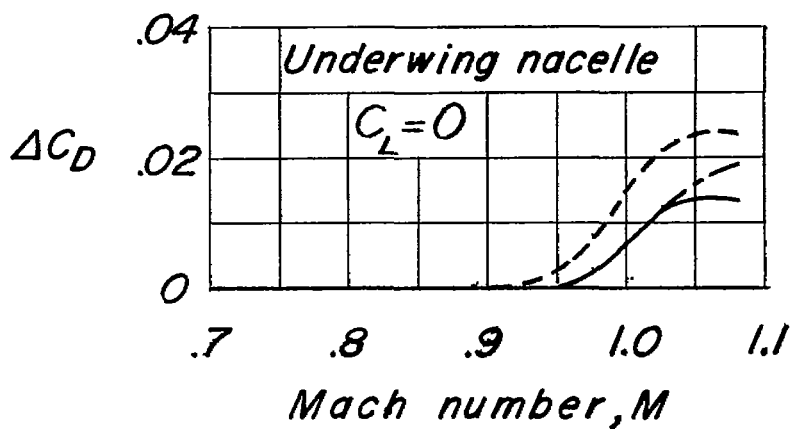


Figure 13.- Variation of nacelle drag coefficient with nacelle spanwise location.

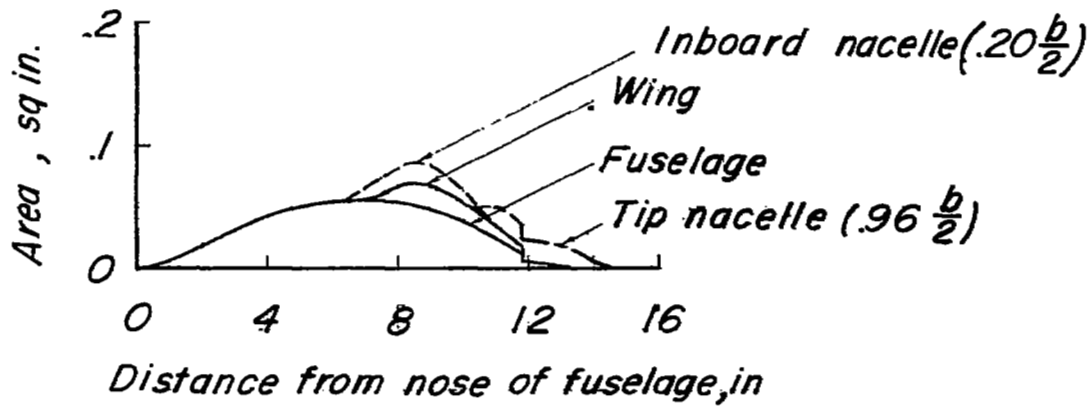


$$\Delta C_D = (C_D)_{M \geq .90} - (C_D)_{M = .90}$$

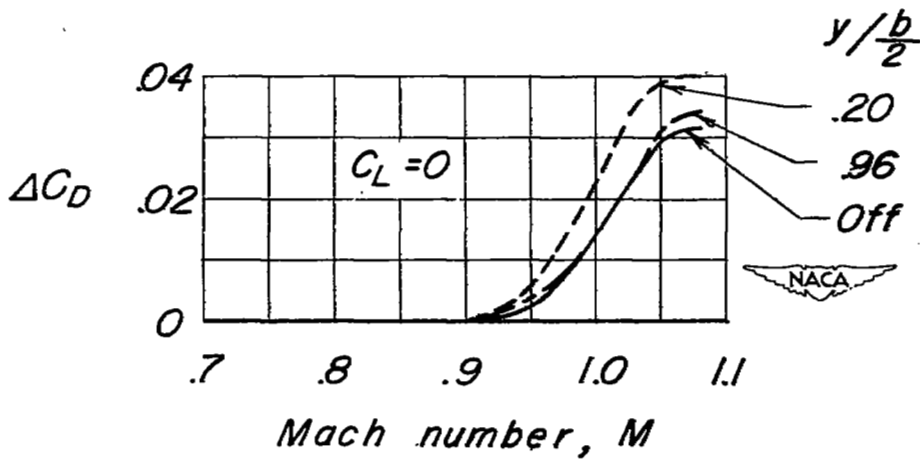


(a) Wing without fuselage.

Figure 14.- Variation of the increment in drag coefficient with Mach number.



$$\Delta C_D = (C_D)_{M \geq .90} - (C_D)_{M = .90}$$



(b) Wing-fuselage combination, symmetrical nacelle.

Figure 14.- Concluded.

Model Config.	Nacelle Vertical Location	Facility		
		Tunnel	Flight	
Wing alone	Symmetrical	—○—		—●—
Wing alone	Underwing	—□—		—●—
Wing fuselage	Symmetrical	—△—	(Ref 3)	—●—
Wing fuselage	Underwing	—◇—	(Ref 5)	—●—

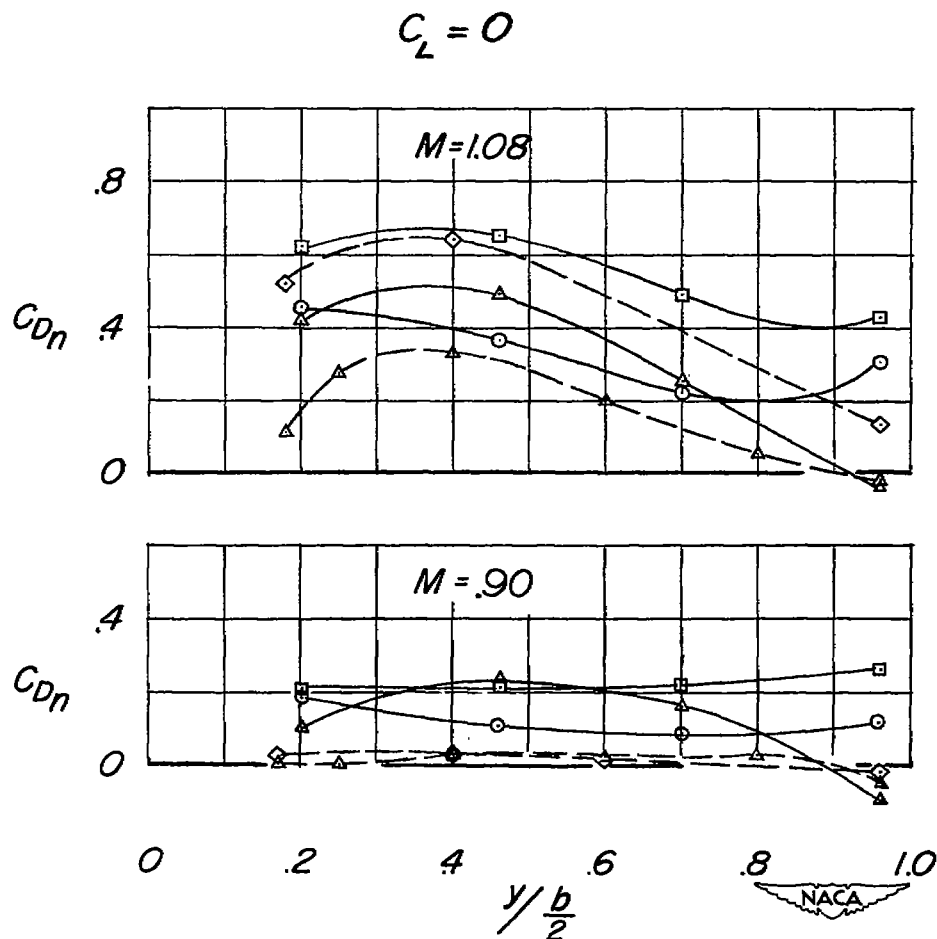
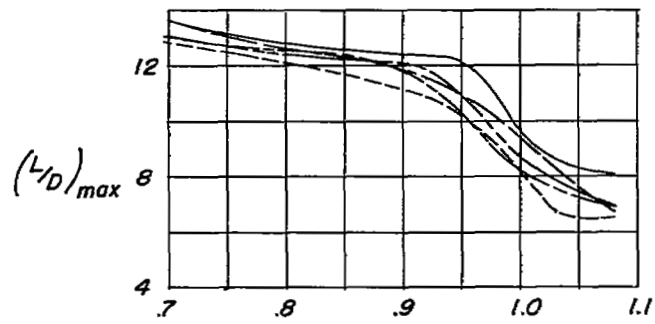
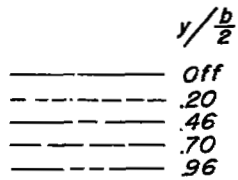
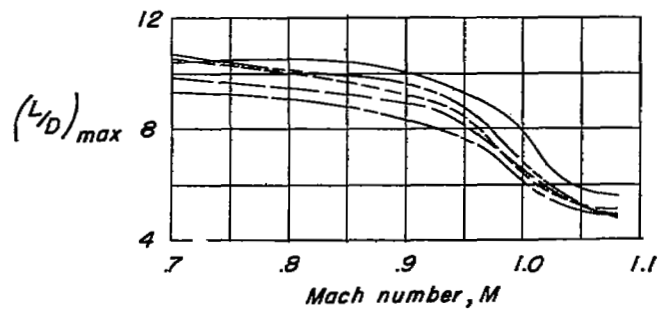


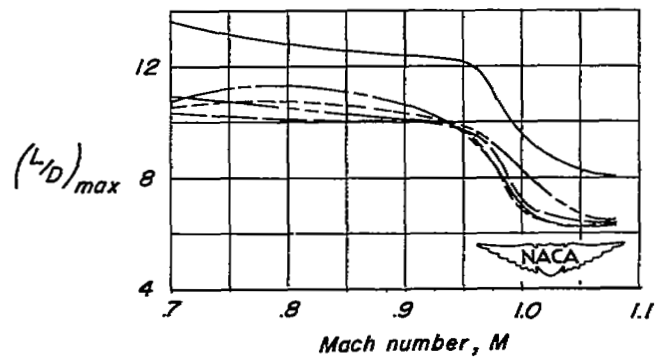
Figure 15.- Comparison between nacelle drag coefficient obtained on the semispan tunnel model and complete models in flight.



Wing alone , symmetrical nacelle



Wing - fuselage , symmetrical nacelle



Wing alone , underwing nacelle

Figure 16.- Variation of the maximum lift-drag ratios with Mach number.

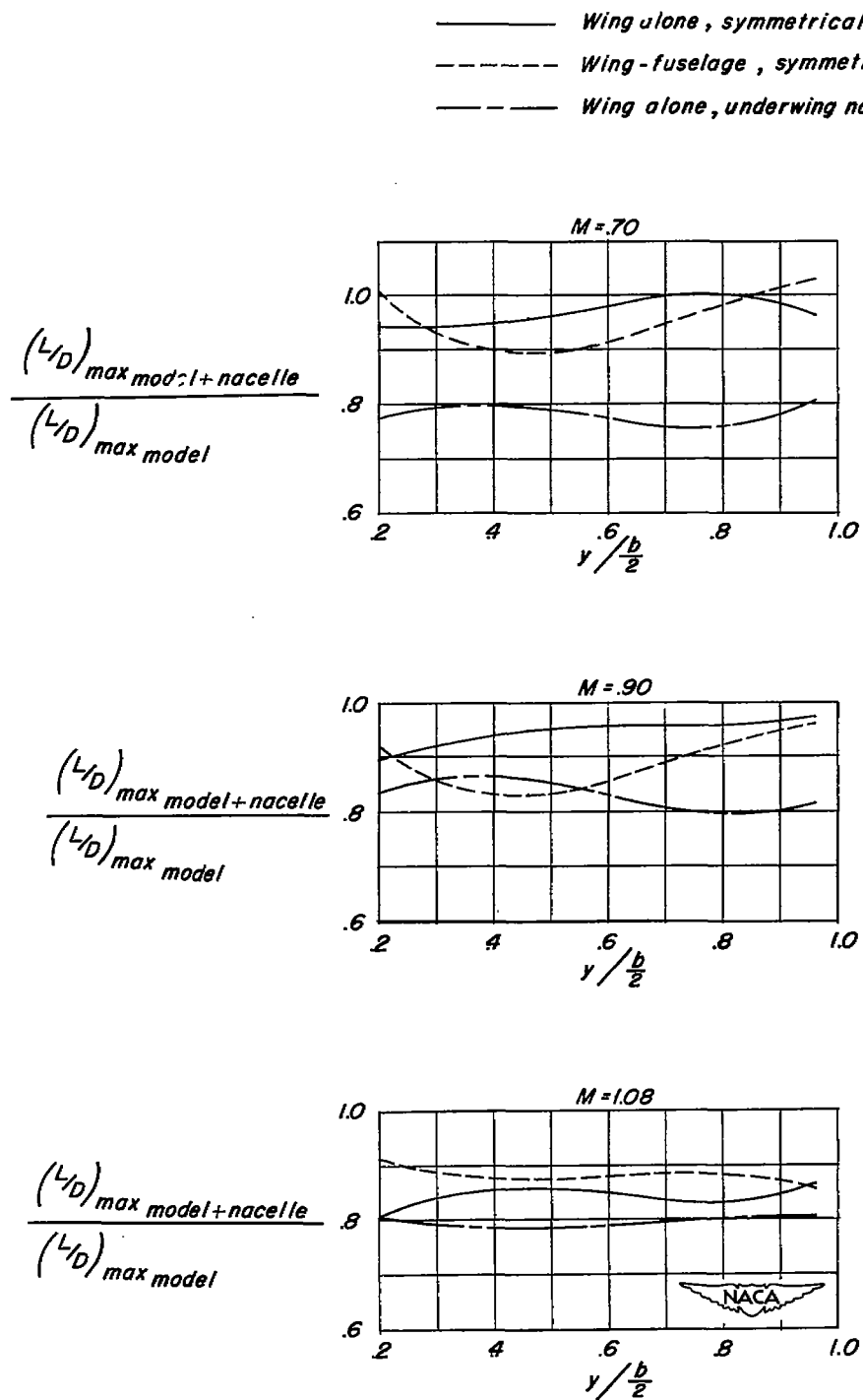


Figure 17.- Variation with nacelle spanwise location of the ratios of the maximum lift-drag ratio of the model with nacelles to the maximum lift-drag ratio of the model without nacelles.

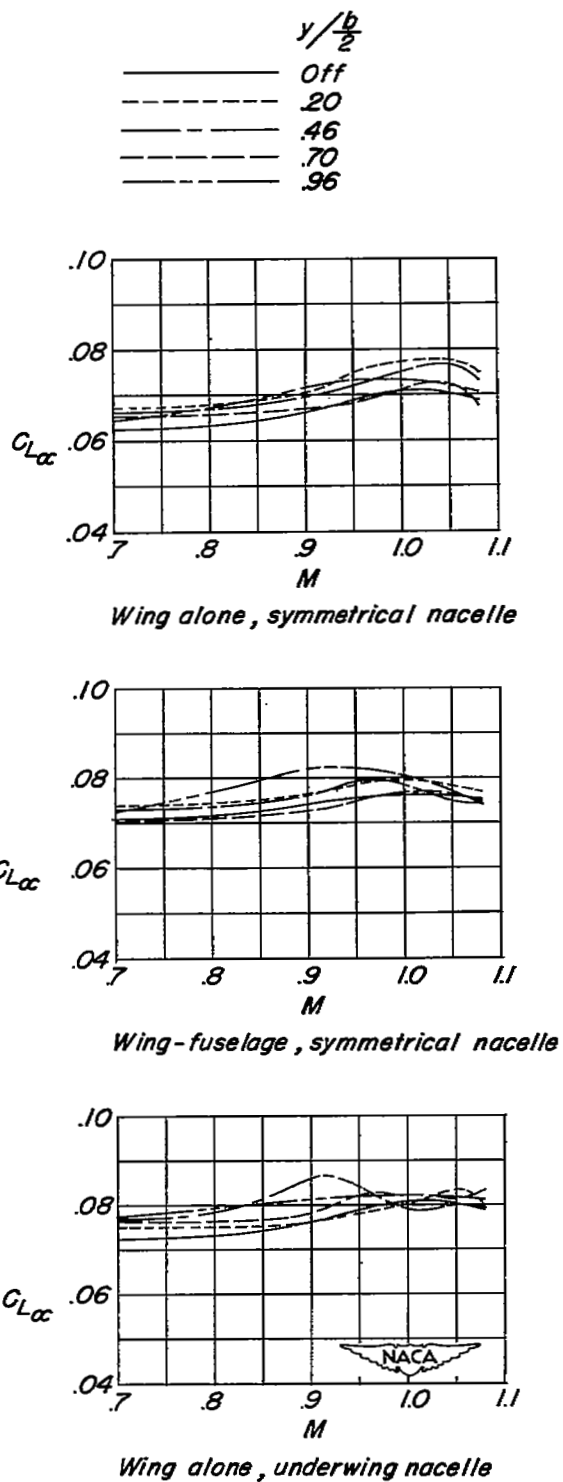


Figure 18.- Variation of the lift-curve slopes with Mach number.

————— *Wing alone, symmetrical nacelle*
 - - - - - *Wing - fuselage, symmetrical nacelle*
 — · — · — *Wing alone, underwing nacelle*

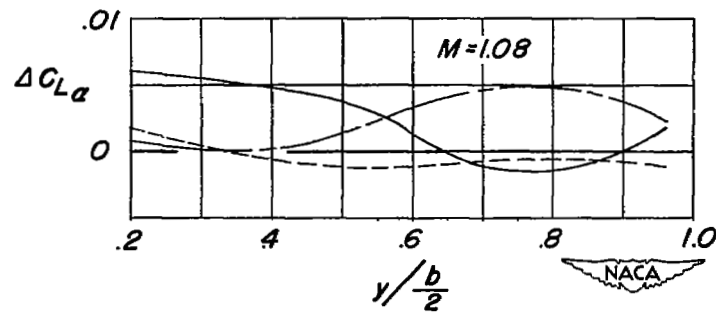
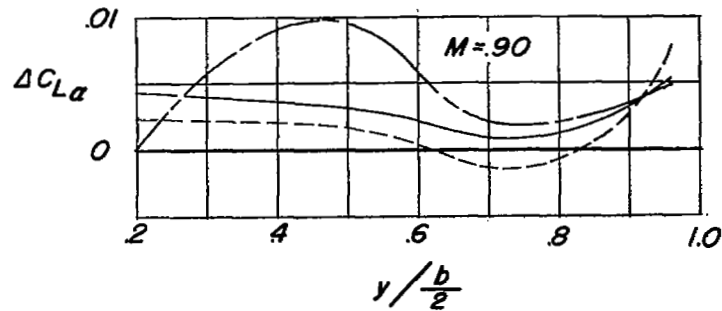
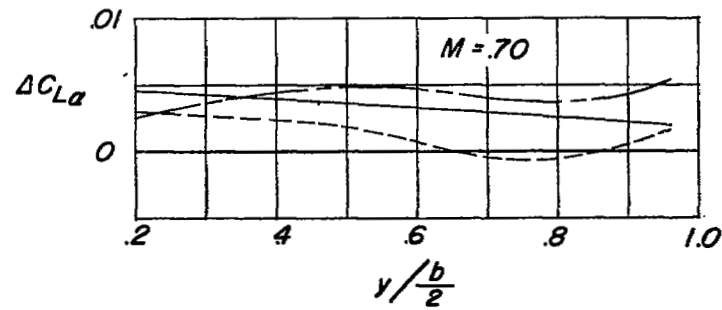
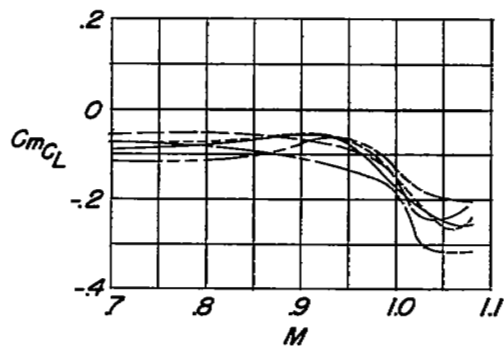
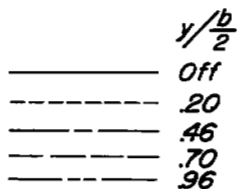
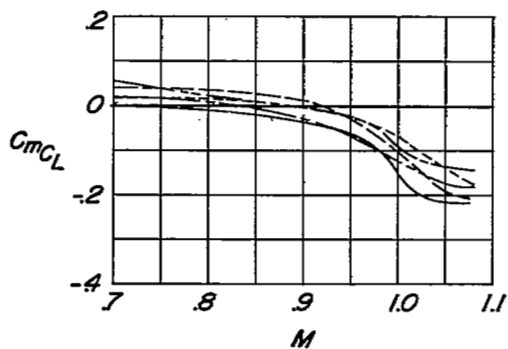


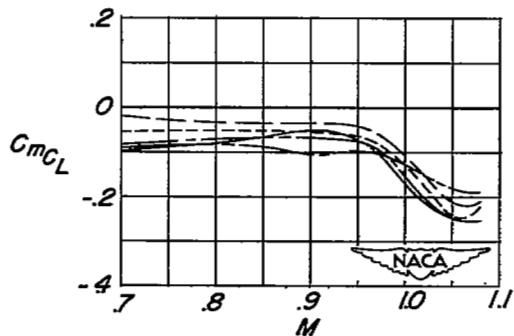
Figure 19.- Variation of the increments in lift-curve slope with nacelle spanwise location.



Wing alone, symmetrical nacelle



Wing-fuselage, symmetrical nacelle



Wing alone, underwing nacelle

Figure 20.- Variation of the pitching-moment-curve slope with Mach number.
 $C_L = 0.1$.

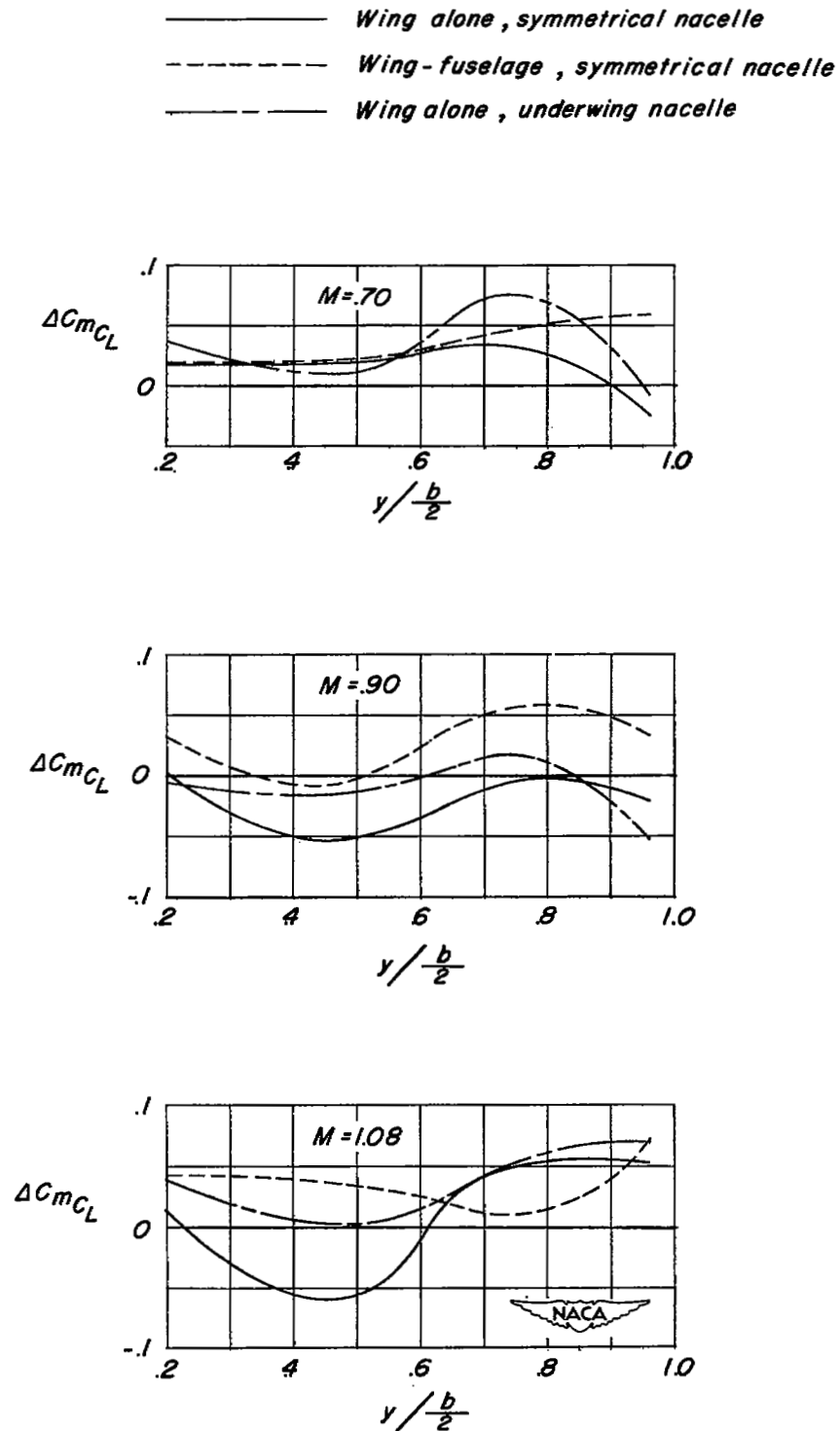


Figure 21.- Variation of the increments in pitching-moment-curve slope with nacelle spanwise location. $C_L = 0.1$.

y/b
 $\frac{y}{2}$

_____ Off
 - - - - - .20
 _____ .46
 - - - - - .70
 _____ .96

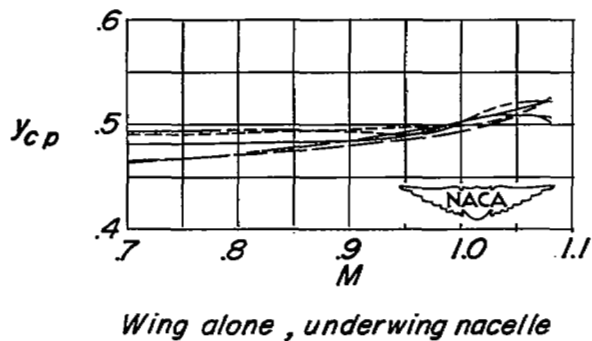
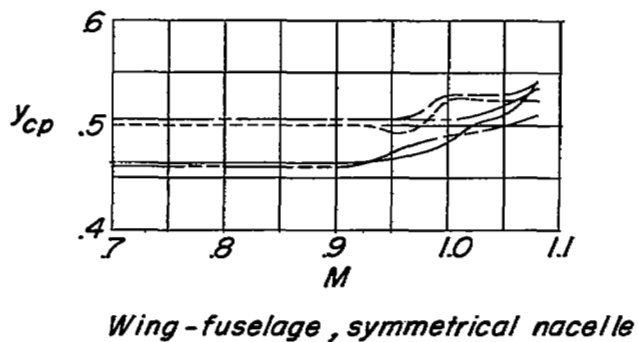
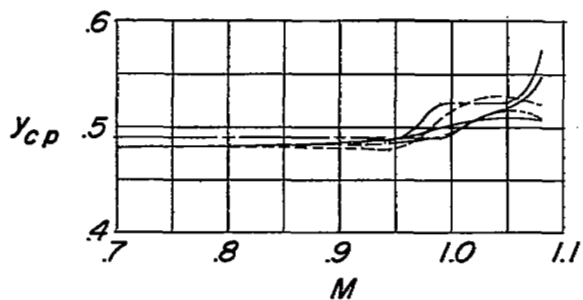


Figure 22.- Variation of the lateral-center-of-pressure locations with Mach number.

_____ *Wing alone, symmetrical nacelle*
 - - - - - *Wing - fuselage, symmetrical nacelle*
 - - - - - *Wing alone, underwing nacelle*

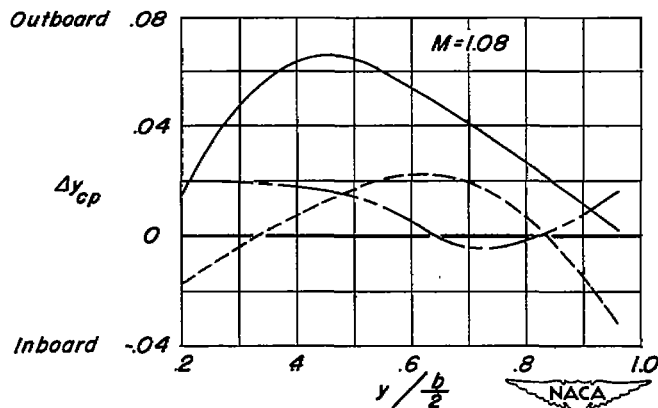
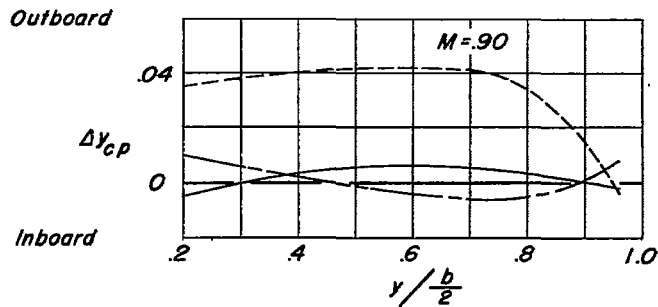
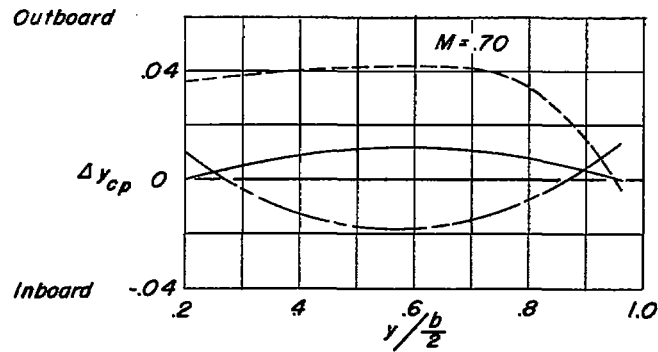


Figure 23.- Variation of the increments of the lateral-center-of-pressure locations with nacelle spanwise location.

SECURITY INFORMATION

NASA Technical Library



3 1176 01438 0084

